This article has been accepted for publication in a future issue of this journal, but has not been fully edited. Content may change prior to final publication.
Citation information: DOI: 10.1109/TNSE.2025.3528768, IEEE Transactions on Network Science and Engineering

Velocity-Adaptive Access Scheme for Semantic-Aware Vehicular Networks: Joint Fairness and AoI Optimization

Xiao Xu, Qiong Wu, *Senior Member, IEEE*, Pingyi Fan, *Senior Member, IEEE*, Kezhi Wang, *Senior Member, IEEE*, Nan Cheng, *Senior Member, IEEE*, Wen Chen, *Senior Member, IEEE*, and Khaled B. Letaief, *Fellow, IEEE*

***Abstract*—In this paper, we address the problem of fair access and Age of Information (AoI) optimization in 5G New Radio (NR) Vehicle to Everything (V2X) Mode 2. Specifically, vehicles need to exchange information with the road side unit (RSU). However, due to the varying vehicle speeds leading to different communication durations, the amount of data exchanged between different vehicles and the RSU may vary. This may poses significant safety risks in high-speed environments. To address this, we define a fairness index through tuning the selection window of different vehicles and consider the image semantic communication system to reduce latency. However, adjusting the selection window may affect the communication time, thereby impacting the AoI. Moreover, considering the re-evaluation mechanism in 5G NR, which helps reduce resource collisions, it may lead to an increase in AoI. We analyze the AoI using Stochastic Hybrid System (SHS) and construct a multi-objective optimization problem to achieve fair access and AoI optimization. Sequential Convex Approximation (SCA) is employed to transform the non-convex problem into a convex one, and solve it using convex optimization. We also provide a large language model (LLM) based algorithm. The scheme's effectiveness is validated through numerical simulations.**

***Index Terms*—Fairness, AoI, Access, Vehicular Networks.**

This work was supported in part by Jiangxi Province Science and Technology Development Programme under Grant No. 20242BCC32016, in part by the National Natural Science Foundation of China under Grant No. 61701197 and 62531015, in part by the Basic Research Program of Jiangsu under Grant BK20252084, in part by the National Key Research and Development Program of China under Grant No. 2021YFA1000500(4), in part by the Shanghai Kewei under Grant 24DP1500500, in part by the Research Grants Council under the Areas of Excellence Scheme under Grant AoE/E-601/22-R and in part by the 111 Project under Grant No. B23008.

Xiao Xu and Qiong Wu are with the School of Internet of Things Engineering, Jiangnan University, Wuxi 214122, China, and also with the School of Information Engineering, Jiangxi Provincial Key Laboratory of Advanced Signal Processing and Intelligent Communications, Nanchang University, Nanchang 330031, China (e-mail: xuxiao@stu.jiangnan.edu.cn, qiongwu@jiangnan.edu.cn). (Corresponding author: Qiong Wu.)

Pingyi Fan is with the Department of Electronic Engineering, State Key laboratory of Space Network and Communications,Beijing National Research Center for Information Science and Technology, Tsinghua University, Beijing 100084, China (email: fpy@tsinghua.edu.cn).

Kezhi Wang is with the Department of Computer Science, Brunel University, London, Middlesex UB8 3PH, U.K. (email: Kezhi.Wang@brunel.ac.uk)

Nan Cheng is with the State Key Laboratory of ISN and the School of Telecommunications Engineering, Xidian University, Xi'an 710071, China (e-mail: dr.nan.cheng@ieee.org).

Wen Chen is with the Department of Electronic Engineering, Shanghai Jiao Tong University, Shanghai 200240, China (e-mail: wenchen@sjtu.edu.cn).

Khaled B. Letaief is with the Department of Electrical and Computer Engineering, the Hong Kong University of Science and Technology, Hong Kong (e-mail: eekhaled@ust.hk).

I. Introduction

With the advancement of vehicular networks, the update speed of vehicular applications has significantly accelerated [1], [2]. Intelligent driving technologies is one of the most important technologies [3]. However, the massive computational tasks generated by these applications and technologies pose great challenges to vehicles with limited computing resources [4], [5]. Moreover, in high-speed environments, the lack of timely information and communication delays can be dangerous. To address this, vehicles use Mobile Edge Computing (MEC) to communicate with Road Side Units (RSUs) to get exact information in a timely manner [6].

Vehicular applications are no longer limited to text data transmission. Instead, they often involve image data [7], [8]. Intelligent driving technologies require vehicles to collect environmental information via onboard sensors, such as high-definition cameras [9]. Transmitting large volumes of image data to the RSU can be time-consuming, and semantic communication has emerged as one potential solution [10], [11].

The goal of communication is to allow the receiver to understand the sender's intent [12]. Semantic communication achieves this by extracting semantic information from the sender's data and transmitting only that. In image semantic systems, semantic information is extracted from images and transmitted as textual information, which avoids transmitting the entire image and focuses on transmitting the core content. Therefore, introducing semantic communication systems into vehicular networks can greatly reduce the difficulty of data transmission and the Age of Information (AoI).

Currently, vehicles use the 5G New Radio (NR) Vehicle to Everything (V2X) protocol introduced in 3GPP Release 16 for data transmission [13]. This protocol has two modes: Mode 1 and 2. Compared to Mode 1, Mode 2 does not require full network coverage, making it more flexible and better suited for vehicle to RSU communication. Hence, vehicles typically use the scheduling-based Semi-Persistent Scheduling (SPS) mechanism in Mode 2 for resource allocation [14], [15].

However, in real-world vehicular networks, RSU coverage is limited, and vehicle speeds often differ across lanes. As a result, vehicles at different speeds spend different amounts of time within the RSU's communication range, leading to unequal opportunities for data exchange. Faster vehicles may receive less useful information than slower ones, which can

pose risks when all vehicles are operating in the same region.

Additionally, Mode 2 introduces a re-evaluation mechanism which allows vehicles to reassess resources after initial selection to avoid collisions [16]. While this mechanism reduces conflicts, the change in transmission time may increase the AoI-critical metric in high-speed vehicular environments [17], [18]. Unlike traditional latency metrics, AoI measures the staleness of data at the receiver relative to its latest generation time, which more directly reflects the effectiveness of status updates. In high-speed mobile environments, once perceived information becomes outdated, it may lead to safety risks such as braking delays, obstacle-avoidance failures, or inaccurate trajectory planning. Therefore, AoI has become a key metric that must be emphasized.

In this work, we define a fairness index for semantic image communication systems and dynamically adjust each vehicle's selection window size according to its velocity to realize fairness access. Meanwhile, considering how selection window adjustments and the re-evaluation mechanism influence AoI, we model AoI using a Stochastic Hybrid System (SHS). We construct a multi-objective optimization task, then solve it using Sequential Convex Approximation (SCA) method and Large Language Model (LLM) based multi-Objective Evolutionary Algorithm based on Decomposition (MOEA/D). As far as we know, no existing work has comprehensively considered both fair access in semantic image systems and the re-evaluation mechanism's influence on AoI, which serves as the motivation for this work.

This paper makes the following key contributions[1]:

1) We consider the fair access problem caused by speed differences in a semantic image communication system. A fairness index is defined to measure access fairness, and selection window sizes are tuned according to vehicles' velocity to achieve fairness access.
2) We analyze how changes in the selection window affect AoI, while also considering the unique re-evaluation mechanism of 5G NR. Using an SHS model, we characterize the relationship between AoI and the selection window size under re-evaluation.
3) We design a multi-objective optimization task to optimize fair access and AoI by dynamically adjusting selection windows based on speed. We propose two algorithms, including SCA and LLM-based MOEA/D, to accommodate optimization needs in different scenarios. During periods of low vehicle density, SCA offers strict mathematical interpretability and thus achieves higher performance in small-scale settings. In high-density scenarios, where conventional evolutionary operators tend to be unstable and hand-crafted operators are difficult to design, we employ LLM-based MOEA/D algorithm, leveraging LLM's reasoning capabilities can better evolve optimal solutions.

The paper is organized as follows: Section II covers related work. Section III outlines the system model, while Section IV presents the definition of the fairness index. Section V models the AoI. Section VI constructs a multi-objective optimization problem and slove it. Section VII analyzes the numerical simulation results. Section VIII concludes the paper.

[1]Source code can be found at : https://github.com/qiongwu86/Velocity-Adaptive-Access-Scheme-for-Semantic-Aware-Vehicular-Networks-Joint-Fairness-and-AoI

II. Related Works

A. Fairness access

We first review the previous work related to fair access. Fair access refers to the situation in a shared wireless communication resource pool where the system, through specific scheduling and resource allocation mechanisms, ensures that different users within the network can obtain relatively reasonable transmission opportunities and resource shares based on their dynamically changing communication needs. In [19], Trung *et al.* achieved fairness among all users in a distributed joint sensing and communication (JSC) system by optimizing the bandwidth allocation between the sensing and communication functions of the JSC nodes. In [20], Fidan *et al.* analytically addressed the max-min fairness problem in Software-Defined Radio Access Networks (SD-RANs) and proposed solutions for two conditions: one aiming to provide max-min fairness for all network users , and the other targeting max-min fairness in terms of throughput both base stations and users. In [21], Wang *et al.* investigated multi-user multiple-input multiple-output (MIMO) technology for licensed spectrum sharing, proposing a fair spectrum allocation scheme between two mobile network operators in a multi-cell, multi-user MIMO network. Fairness is maintained by allocating spectrum to each operator in proportion to its contribution. None of the above works have considered the fair access in vehicular networks.

B. Age of information

We continue to review related work on AoI under 5G NR. AoI is a performance indicator that measures the obsolescence or freshness of information. That is, the time elapsed from the generation moment of the latest successfully received data packet at the receiving end to the current observation moment. In [22], Rolich *et al.* pointed out that while SPS improves resource utilization efficiency, it does not consistently enhance AoI performance. They revealed the fundamental trade-off between reliability (PDR) and timeliness (AoI), emphasizing the need for careful persistence management in vehicular communication systems. In [23], Alexey *et al.* developed an SPS parameter adaptation method aimed at reducing the average AoI of cooperative awareness messages. Built upon analytical modeling of SPS, the method's performance is validated via simulation. In [24], Ekaterina *et al.* analyzed the influence of 5G NR system configurations on application-level AoI performance. To achieve this, they used queuing theory and stochastic geometry tools to quantify the mean and distribution of PAoI and sojourn time, taking into account traffic arrival patterns and the coefficient of variation and auto-correlation in service characteristics within the 5G NR system. In [25], Wang *et al.* noted that conventional broadcast-based data dissemination often leads to congestion, as it requires participation from a large number of vehicles, thereby resulting in a higher AoI. To address this, they leveraged mobile edge computing and proposed a new unicast-based dissemination

method to reduce AoI. In [26], Song *et al.* discussed the joint optimization of AoI and energy consumption in 5G NR and employed Deep Reinforcement Learning (DRL) to address the problem. However, they did not provide an discussion on AoI modeling or the impact of the re-evaluation mechanism. In recent years, both 5G NR and semantic communication have witnessed rapid development. In [27], Rolich *et al.* based on 5G NR-V2X Mode 2, proposed an algorithm that adaptively adjusts SPS parameters to minimize AoI. In [28] Shao *et al.* introduced a semantic-aware resource allocation method aimed at reducing information latency. Nevertheless, existing AoI studies generally overlook or only qualitatively describe the newly introduced re-evaluation mechanism in NR Release 16, resulting in AoI models that fail to accurately reflect the actual transmission dynamics of NR-V2X Mode 2.

We incorporates state transitions and rate processes of the re-evaluation mechanism into the AoI mathematical model within the SHS framework, establishing a more comprehensive and standards-compliant AoI analytical framework than prior research. Additionally, existing studies have not adequately addressed the issue of access fairness arising from vehicles with different speeds. The fairness and the adaptive selection window optimization based on vehicle speed proposed in this paper achieve the joint optimization of fairness and AoI, which fills the critical gap in the current researches.

C. Joint optimization

We review the articles related to jointly optimizing AoI and fair access. In [29], Xu *et al.* considered the joint optimization of fair access and AoI under a preemption mechanism by adjusting the selection window size. In [30], Wan *et al.* considered the fair access and AoI optimization for vehicle in the 802.11p simultaneously, and designed a scheme that dynamically tunes the contention window (CW) based on speed in order to achieve fair access and optimize AoI, and finally adopted a heuristic algorithm to solve the problem. In [31], Wu *et al.* also addressed the issues of fair access and AoI for vehicle nodes under the IEEE 802.11p protocol, and employed an extended Deep Q-learning (DQN) method to allocate optimal CW values for the nodes.

However, [30], [31] only addressed fair access and joint optimization under the IEEE 802.11p protocol, which is no longer applicable in today's 5G NR V2X protocol. Furthermore, while [29] took into account the preemption mechanism in 5G NR, it did not evaluate another unique mechanism—the re-evaluation mechanism—nor did it consider the fairness index in an image semantic communication system.

In summary, existing research can be categorized into three groups. First, studies focusing on fairness are mostly conducted in non-NR scenarios and fail to account for semantic communication systems and the dynamics of information age. Second, research on AoI lacks explicit AoI modeling that incorporates both selection window size and the re-evaluation process, and has not explored co-optimization with fair access in semantic communication systems. Third, studies that jointly consider fair access and AoI are primarily limited to the IEEE 802.11p communication protocol, or do not consider the impact of the re-evaluation mechanism in 5G NR, nor do they address the influence of semantic communication systems.

III. System Model

In this section, we introduce the system model, including the scene model, and two models that determine the overall process from the generation to the transmission of semantic information: the semantic model and the SPS model.

A. Scenario Model

As shown in Fig. 1, we focus on a multi-lane highway scenario comprising N lanes. RSUs equipped with computationally capable servers, are positioned along the roadside. The number of vehicles covered by an RSU is set as N_v. Upon entering the communication range of an RSU, vehicles attempt to establish communication with it. This paper specifically focuses on the scenario where vehicles transmit images to the RSU. Typically, vehicles exchange data with the RSU via the 5G NR Vehicle to Infrastructure (V2I) Mode 2 protocol. Given the large data volumes associated with image transmission, semantic communication is employed to reduce the amount of transmitted data. Since the scenario we are considering is a highway scenario, and given that each lane has its own speed limit, the vehicle's speed typically fluctuates within a relatively narrow range. Moreover, the communication time within the RSU coverage time scale is usually only a few seconds. Therefore, in our model, the vehicle's speed can be regarded as constant. Meanwhile, vehicles in adjacent lanes exhibit a speed difference of at least 3.6 m/s. Similar to [30], we only consider the uplink, since the main data in this scheme originates from the semantic information uploaded by vehicles via the uplink. Compared with the uplink, the downlink only transmits a minimal amount of control signaling or acknowledgment messages, with very little useful information. Furthermore, given that the downlink in NR has more stable channel conditions [13], it does not impose constraints in this scheme and does not affect the analysis. Therefore, only the uplink is considered.

B. Semantic Model

Next, we introduce the semantic model. The role of the semantic model is to transform images into semantic information, which determines the information that needs to be transmitted in the system.

Following the model in [32], we categorize semantic information into nodes and the relationships between nodes. Each node represents an object, such as a vehicle, pedestrian, etc. The image's semantic data can be decomposed into multiple semantic triples. A semantic triple can be represented as: [Vehicle 1] [in front of] [Vehicle 2]. Here, vehicle 1 and vehicle 2 are two nodes, and is in front of denotes the relationship between them. Consequently, multiple semantic triples can be used to describe a single image. We employ the scene graph extraction model proposed in [33] to obtain semantic information from the raw images captured by vehicles. This extracted semantic information is then transmitted in the form

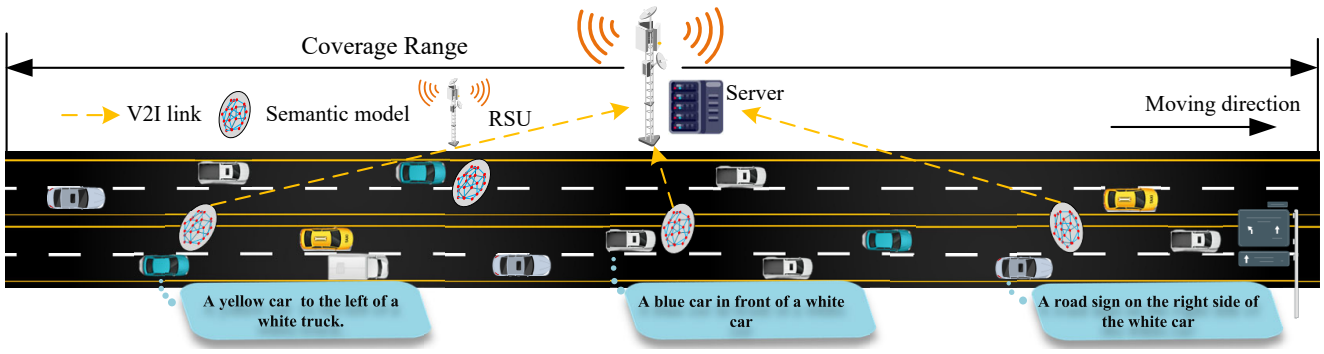

Fig. 1: Scenario Model

of triples. The semantic triples corresponding to image I_k transmitted by vehicle v can be represented as:

$$S_{vk} = \left\{ s_{vk}^1, s_{vk}^2, \cdots, s_{vk}^n, \cdots, s_{vk}^{N_{vk}} \right\}, \tag{1}$$

where $s_{vk}^n = \left(o_{vk,i}^n, r_{vk,ij}^n, o_{vk,j}^n \right)$, where o_i and o_j denote objects i and j in image k, respectively, and r_{ij} describes the relationship between objects i and j. We remark that $r_{ij} \neq r_{ji}$ due to the directional nature of relationships. N_{vk} denotes the quantity of semantic triples in image k. Thus, a semantic triple s can be formally defined as $s = (o_i, r_{ij}, o_j)$, and the collective set $S = \{s_1, s_2, ..., s_{N_{vk}}\}$ constitutes the complete semantic representation of an image.

To quantify the data volume of semantic information, $L(x)$ was defined as the character count in a triple component x. Consequently, the semantic data volume for image I_k transmitted by vehicle v is given by:

$$L(S_{vk}) = \sum_{n=1}^{N_{vk}} \left(Z(o_{vk,i}^n) + Z(r_{vk,ij}^n) + Z(o_{vk,j}^n) \right). \tag{2}$$

The communication quality of a semantic communication system is an important factor influencing the effectiveness of access schemes. A widely used metric for measuring communication quality is semantic similarity. When vehicles are far apart or there is significant interference or noise, the communication often suffers, leading to errors in semantic information extraction or failure to extract it at all. This causes fluctuations in semantic similarity. Following [32], we adopt an image-to-graph semantic similarity metric, defined as:

$$\xi(S_{vk}, G_{vk}) = \frac{\left\| \sum_{n=1}^{N_{vk}} \overline{D(s_{vk}^n)} D(G_{vk})^T \overline{D(s_{vk}^n)} \right\|}{\| D(G_{vk}) \|}, \tag{3}$$

where $D(\cdot)$ denotes the vectorization function of a pre-trained Deep Neural Network (DNN), then orthogonalize it as $\overline{D(\cdot)}$ by the GramSchmidt algorithm. Through this pre-trained DNN, we obtain the vectorized semantic data and the image. To compute the semantic similarity in Eq.3, the images and triples need to be mapped into a unified semantic vector space. We employ a DNN-based semantic encoder to map objects , relationships, and images into the same semantic vector space [33]. The reason is that DNNs can extract high-level semantic features to represent both images and semantic triples [32], [34]. Meanwhile, since the embeddings output by DNNs are usually non-orthogonal, we apply Gram–Schmidt orthogonalization to stabilize the inner-product similarity calculation, avoiding bias caused by feature correlations. Gram–Schmidt orthogonalization is a standard vector preprocessing method in machine learning and signal processing [32], [35].

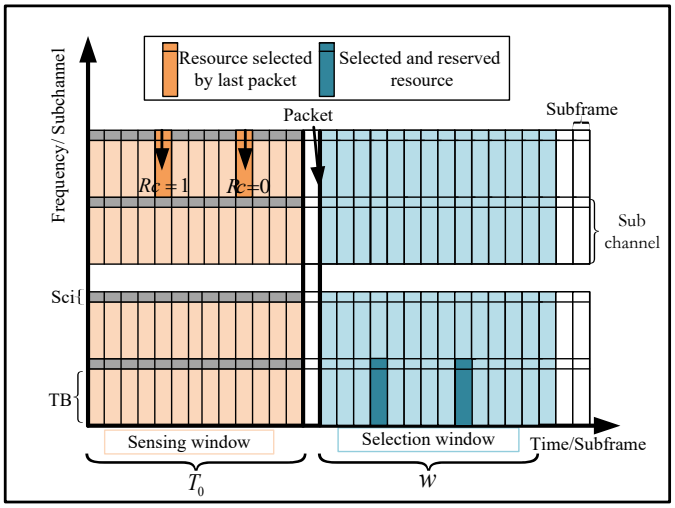

Fig. 2: SPS Model

C. SPS Model

Through the semantic model, we have obtained the semantic information that needs to be transmitted. Next, we will introduce how to use the SPS model to determine how to schedule resources to transmit the semantic information obtained from the semantic model.

In accordance with the V2X protocol specified in 3GPP Release 16, vehicles typically perform resource allocation and communicate with other devices. Similar to Mode 4 in LTE-V2X, vehicles operating in Mode 2 of 5G NR can autonomously allocate resources from the communication resource pool without network assistance. Under Mode 2, vehicles typically employ a SPS scheme for resource scheduling. As illustrated in Fig. 2, communication resources are divided into multiple subchannels in the frequency domain. Each subchannel consists of a Scheduling Control Information (SCI) field and a transport channel, where SCI carries control information and the transport channel transmits Transport Blocks (TBs). A vehicle reserves a subchannel based on its Resource Reservation Interval (RRI) for transmitting its next data packet. When selecting a new resource, the vehicle enters an exclusion

TABLE I: Important Symbols

Symbol	Description
V_v	Vehicle v's speed.
N_v	The number of vehicles.
R	RSU's communication range.
G_{max}	Maximum iteration number.
RRI	Source selection interval.
B	Bandwidth.
μ	Subcarrier spacing factor.
V_{min}	The lower bound of vehicle's speed.
V_{max}	The upper bound of vehicle's speed.
I_v	The expected data volume transmitted by vehicle v.
P_v	The number of images transmitted by vehicle v
D_p	The average successfully transmitted data size per image.
T_v^{dw}	Vehicle v's dwell time within the RSU's coverage area.
T_v^{tx}	The average transmission time per image for vehicle v.
p_v	Vehicle v's power.
PR_v	The successful communication probability between vehicle v and the RSU.
$\delta_{v,j}$	The transmission collision probability.
B_l	The number of bits per transmitted character.
ISS_v	The average semantic similarity for vehicle v.
h_v	The channel gain between vehicle v and the RSU.
G_{fair}^v	The fairness index of vehicle v.
G_{fair}	The averaged network's fairness.
$\boldsymbol{A(t)}$	The set of current AoI.
$S(t)$	The current link state.
$A_r(t)$	The AoI of the data stored at the RSU.
$A_v(t)$	The AoI at link v.
$\boldsymbol{\psi_l}$	The transition mapping matrix for l.
η_l	The transition rate of l.
R_v	The average transmission failure probability.
H_v	The average service probability.
E_v	The average re-evaluation probability.
$\boldsymbol{Q}_{sl}$	The steady state correlation.
Δ_k	The AoI of link k .
$\boldsymbol{b_s}$	A binary differential vector coefficient.
$\bar{\pi}_s$	The steady-state probability of state s.

phase within a selection window, utilizing resource information obtained during a sensing window. During this exclusion phase, the vehicle must exclude resources already reserved by other vehicles or those whose SCI-indicated Reference Signal Received Power (RSRP) exceeds a predefined threshold. After exclusion, the vehicle chooses a resource at random from the remaining available resource list for communication.

Notably, unlike LTE V2X, NR V2X introduces a novel mechanism — the re-evaluation mechanism. Upon adopting this mechanism, a vehicle continues sensing resource information during the original selection window. If the vehicle detects that its selected resource becomes unavailable, it defines a new selection window, performs the resource exclusion procedure again, and subsequently selects a new resource.

IV. Fairness Index

This section considers the transmission rate, semantic similarity, and transmission collision probability under 5G NR in an image semantic communication system, and establishes a fairness index to assess the extent to which vehicles achieve fair access. The important parameters employed in this paper are listed in Table I.

A. Transmission rate

Fair access implies that the data volume transmitted by each vehicle should be comparable. Since vehicles transmit numerous images during operation, we have:

$$E(I_v) = C, \tag{4}$$

where I_v denotes the expected data volume transmitted by vehicle v. Due to probabilistic transmission failures and slight variations in the semantic information size across images, we consider the expected value. C is a constant. Furthermore, I_v can be expressed as:

$$I_v = P_v \cdot D_p, \tag{5}$$

where P_v refers to the total images sent by vehicle v. D_p denotes the average successfully transmitted data volume per image. P_v can be further expressed as:

$$P_v = \frac{T_v^{dw}}{T_v^{tx}}, \tag{6}$$

where T_v^{dw} denotes the period vehicle v remains under the RSU's coverage. T_v^{tx} represents the average transmission time per image for vehicle v. T_v^{dw} is given by:

$$T_v^{dw} = \frac{R}{V_v}, \tag{7}$$

where R denotes RSU's coverage. V_v denotes vehicle v's speed. T_v^{tx} can be expressed as:

$$T_v^{tx} = \frac{I}{B \cdot \log_2(1 + \frac{p_v \cdot h_v \cdot {d_v}^{-\partial}}{\sigma^2}) \cdot PR_v}, \tag{8}$$

where p_v represents vehicle v's power, h_v indicates the channel gain between vehicle v and the RSU, d_v denotes their separation distance, α denotes the path loss exponent, σ^2 signifies the noise power, PR_v represents the successful communication probability between vehicle v and the RSU, and I denotes the number of bits per image, B denotes the bandwidth. According to [36], the channel model adopts an autoregressive model, i.e.:

$$h_v = \rho_v {h_v}' + e\sqrt{1-\rho_v^2}, \tag{9}$$

where ρ_v is the autocorrelation coefficient, ${h_v}'$ denotes the channel gains from the preceding slot, with e following a Gaussian distribution.

B. Successful receiving probability

We now discuss PR_v. Assuming all vehicles support full-duplex communication, PR_v can be expressed as:

$$PR_v = \prod_{j \neq v} (1 - \delta_{v,j}), \tag{10}$$

where $\delta_{v,j}$ denotes the transmission collision probability for vehicle v and vehicle j. which denotes that the vehicles experience contention over Physical Resource Blocks (PRBs). Such contention occurs when several transmitters, operating within overlapping time frames, attempt to occupy identical PRBs. Based on [37], $\delta_{v,j}$ is expressed as:

$$\delta_{v,j} = P_O \cdot P_{SH|O} \cdot \frac{C_{Ca}}{N_{Ca}^2}, \tag{11}$$

where P_O quantifies the chance of temporal overlap between the selection windows of distinct vehicles. $P_{SH|O}$ denotes the conditional probability that they select resources from this overlapping region. When an overlap happens, C_{Ca} refers to the number of shared candidate PRBs, and N_{Ca} indicates the mean count of PRBs within the candidate pool. The associated conditional probability P_O is defined as:

$$P_O = \frac{w_v + w_j + 1}{1000 \cdot 2^{\mu} \cdot RRI}, \tag{12}$$

where w_v and w_j indicate the selection window sizes of vehicles v and j, respectively. RRI denotes the interval between consecutive resource selections, and μ is the subcarrier spacing factor. $P_{SH|O}$ is given by:

$$P_{SH|O} = \left(\frac{N_{Sc} \cdot N_{Sh}}{N_r}\right)^2. \tag{13}$$

N_{Sc} represents the total subchannels, and N_{Sh} refers to the resources shared across the overlapped window. N_r denotes the overall resource count. N_{Sh} is defined as:

$$N_{Sh} = \frac{(w_v + 1)(w_j + 1)}{w_v + w_j + 1}. \tag{14}$$

C. Fair index

From Eq. (2), we obtain the semantic information volume per single image. However, vehicles transmit numerous images within the RSU's communication range, which can incur significant latency in high-mobility vehicular environments. To mitigate computational overhead, we precompute the average semantic information volume per image. Consequently, I can be further expressed as:

$$I = \frac{B_l \cdot \sum_{k=1}^{K} L(S_{vk})}{K}, \tag{15}$$

where K denotes the part of images in Visual Genome (VG) dataset [38], and B_l represents the number of bits per transmitted character.

Through Eq. (6), we obtain the number of images vehicle v can transmit within the RSU's communication range. However, since semantic communication is employed, we must ensure the extracted semantic information accurately represents the original images. To evaluate semantic communication quality within the RSU coverage, we define the average semantic similarity for vehicle v as:

$$ISS_v = \frac{\sum_{k=1}^{k=G} \xi(S_{vk}, G_{vk})}{U}. \tag{16}$$

Considering that calculating the similarity of all images may consume extensive computational resources, we set U as the upper limit on the number of similarity calculations. Therefore, the average successfully transmitted data size per image is:

$$D_p = ISS_v \cdot I. \tag{17}$$

Accordingly, Eq. (4) can be restated in the following form:

$$\frac{R \cdot \sum_{k=1}^{k=U} \xi(S_{vk}, G_{vk}) \cdot B \cdot \log_2(1 + \frac{p_v \cdot h_v \cdot {d_v}^{-\partial}}{\sigma^2}) \cdot PR_v}{V_v \cdot U} = C. \tag{18}$$

By transferring parameters unrelated to vehicle v, we obtain:

$$G^v_{fair} = \frac{\sum_{k=1}^{k=U} \xi(S_{vk}, G_{vk}) \cdot \log_2(1 + \frac{p_v \cdot h_v \cdot {d_v}^{-\partial}}{\sigma^2}) \cdot PR_v}{V_v}. \tag{19}$$

Thus, we derive the fairness index G^v_{fair}. Based on Eq.19, we can observe that the fairness index is influenced by multiple factors, especially semantic similarity. When the communication system is affected by interference and communication quality is poor, it often impacts the extraction of semantic information, leading to fluctuations in semantic similarity. As a result, the fairness index also fluctuates. To achieve fair access, the proposed scheme adjusts the selection window size to regulate the impact of communication quality on fair access, ensuring that vehicles with different communication conditions can achieve fair access in the semantic communication system.

The averaged network's fairness can be described as:

$$G_{fair} = \frac{\sum_{v=1}^{N_v} G^v_{fair}}{N_v}. \tag{20}$$

V. Model of AoI

Next, we proceed to analyze the AoI within the RSU's communication range. We define the communication between vehicle v and the RSU as link v, resulting in N_v total links in the network. The transmission model adopts an SHS framework for modeling [39], [40].

Let $S(t)$ denote the current link state and $\boldsymbol{A(t)}$ represent the set of current AoI. Thus, the complete system model is formulated as $(S(t), \boldsymbol{A(t)})$, $S(t) \in \{0, 1, 2, \ldots v, \ldots, N_v\}$, $\boldsymbol{A(t)} = [A_r(t), A_v(t)]$. When $S(t) = 0$, it indicates the current link is idle (no vehicle communicating with RSU). When $s(t) = v$, it means vehicle v is exchanging data with the RSU. $A_v(t)$ represents the AoI of link v at time t, and $A_r(t)$ represents the RSU's AoI. After network setup is complete,

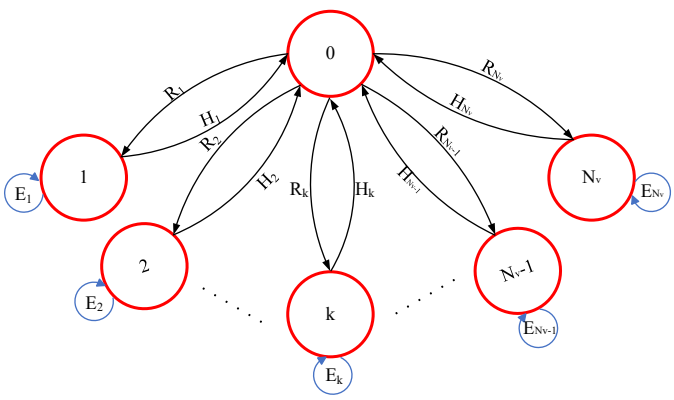

Fig. 3: Markov Model

TABLE II: SHS Transitions model

$\boldsymbol{l}$	$\boldsymbol{s_l \to s'_l}$	$\boldsymbol{\eta_l}$	$\boldsymbol{S' = S\psi_l}$	$\boldsymbol{\psi_l}$	$\boldsymbol{\overline{Q}_{S'_l} = \overline{Q}_{S_l}\psi_l}$
1	$0 \to 1$	R_1	$[A_r, A_v]$	$\begin{bmatrix}1 & 0\\ 0 & 1\end{bmatrix}$	$[\overline{Q}_{00}, \overline{Q}_{01}]$
$\vdots$	$\vdots$	$\vdots$	$\vdots$	$\vdots$	$\vdots$
N	$0 \to N$	R_{N_v}	$[A_r, A_v]$	$\begin{bmatrix}1 & 0\\ 0 & 1\end{bmatrix}$	$[\overline{Q}_{00}, \overline{Q}_{01}]$
$N+1$	$1 \to 0$	H_1	$[A_r, A_v]$	$\begin{bmatrix}1 & 0\\ 0 & 1\end{bmatrix}$	$[\overline{Q}_{10}, \overline{Q}_{11}]$
$\vdots$	$\vdots$	$\vdots$	$\vdots$	$\vdots$	$\vdots$
$N+k$	$k \to 0$	H_k	$[A_v, 0]$	$\begin{bmatrix}0 & 0\\ 1 & 0\end{bmatrix}$	$[\overline{Q}_{k1}, 0]$
$\vdots$	$\vdots$	$\vdots$	$\vdots$	$\vdots$	$\vdots$
$2N$	$N \to 0$	H_{N_v}	$[A_r, A_v]$	$\begin{bmatrix}1 & 0\\ 0 & 1\end{bmatrix}$	$[\overline{Q}_{N0}, \overline{Q}_{N1}]$
$2N+1$	$1 \to 1$	E_1	$[A_r, A_v]$	$\begin{bmatrix}1 & 0\\ 0 & 1\end{bmatrix}$	$[\overline{Q}_{10}, \overline{Q}_{11}]$
$\vdots$	$\vdots$	$\vdots$	$\vdots$	$\vdots$	$\vdots$
$3N$	$N \to N$	E_{N_v}	$[A_r, A_v]$	$\begin{bmatrix}1 & 0\\ 0 & 1\end{bmatrix}$	$[\overline{Q}_{N0}, \overline{Q}_{N1}]$

$A_r(t)$ increases linearly with a slope of one, meaning the AoI at the RSU grows linearly over time. When the RSU receives data from vehicle v, it replaces $A_r(t)$ with the AoI from link v. Meanwhile, the AoI at link v, $A_v(t)$, begins linear growth with a slope of one after the vehicle generates a data packet. Therefore, we can model $S(t)$ as a discrete process and $\boldsymbol{A(t)}$ as a continuous process. Furthermore, transitions in the discrete process cause resets in the continuous process. Moreover, we set l as a transition in the discrete process $S(t)$, and let $\boldsymbol{\psi_l}$ be the transition mapping matrix for l.

Let $\mathbf{A}'$ and $\mathbf{A}$ represent the state of AoI through transition l. Similarly, we define S_l and S'_l to denote the discrete process before and after transition l, while η_l represents the transition rate of l. This can be further categorized into three types of transition rates:

1) Average transmission failure probability R_v, representing the transition rate caused by interference or packet collisions;
2) Average service probability H_v, denoting the average transition rate for successful packet transmissions;
3) Average re-evaluation probability E_v, introduced for vehicle retransmission mechanisms.

Specifically, when transmission fails, the system transitions from state 0 to state v at probability R_v due to retransmission. Upon successful transmission, the system transitions from state v back to idle state 0 at probability H_v. During re-evaluation, the system remains in state v but triggers a re-evaluation at probability E_v.

We define $\bar{\boldsymbol{Q}}_{sl} = [\bar{Q}_{s0}, Q_{s1}]$, where $\bar{Q}_{s0}$ as the steady-state correlation between s_l and A_r, and $\bar{Q}_{s1}$ for s_l and A_v. Accounting for continuous-process resets from discrete transitions: $\bar{\boldsymbol{Q}}' = \bar{\boldsymbol{Q}}_{s'_l} A'$, where $\bar{\boldsymbol{Q}}'$ captures post-transition steady-state correlation. The SHS transition process is summarized in Table II, which classifies transitions into three types: 1. Successful transmission. 2. Failed transmission. 3. Re-evaluation mechanism. Table II lists the transitions:

1) Transition l_1 represents the system state changing from 0 to other states. Taking link v as an example, the idle channel being occupied by link v indicates the previous transmission of link v failed and requires retransmission at probability R_v. Since the transmission failed, the AOI at the RSU remains unchanged and continues its linear growth with slope 1. This transition can be expressed as:
$$\boldsymbol{A'} = \boldsymbol{A} \cdot \boldsymbol{\psi_{l_1}} = [A_r, A_v], \bar{\boldsymbol{Q}}_{sl_1}{}' = \bar{\boldsymbol{Q}}_{sl_1} \cdot \boldsymbol{\psi_{l_1}} = [\bar{Q}_{k1}, 0].$$
2) $l_2 = \{N_v + 1, N_v + 2, N_v + 3, \ldots, 2N_v\}$. The transition l_2 is the change of the system state from other states to 0. Taking link $N_v + k$ as an example, this means that a previously busy channel becomes idle. This indicates that the last transmission on link $N_v + k$ was successful, so no further transmission is required. This transition occurs at a probability of H_k. Meanwhile, since the transmission was successful, the AoI at the RSU is reset to the AoI of link $N_v + k$, and the AoI of link $N_v + k$ is set to zero. Therefore, for this successful transmission, we have:
$$\boldsymbol{A'} = \boldsymbol{A} \cdot \boldsymbol{\psi_{l_2}} = [A_v, 0], \bar{\boldsymbol{Q}}_{sl_2}{}' = \bar{\boldsymbol{Q}}_{sl_2} \cdot \boldsymbol{\psi_{l_2}} = [\bar{Q}_{k1}, 0]$$
For links other than $N_v + k$, the success of any link has no impact on link k's AoI, that is,
$$\boldsymbol{A'} = \boldsymbol{A} \cdot \boldsymbol{\psi_{l_2}} = \boldsymbol{A}, \bar{\boldsymbol{Q}}_{sl_2}{}' = \bar{\boldsymbol{Q}}_{sl_2} \cdot \boldsymbol{\psi_{l_2}} = \bar{\boldsymbol{Q}}_{sl_2}$$
3) Transition $l_3 = \{2N_v + 1, 2N_v + 2, 2N_v + 3, \ldots, 3N_v\}$, The transition l_3 is the transition of the system state from any state other than 0 back to itself. This means that the transmission process has been re-evaluated, but since the transmitted information, sender, and receiver have not changed, only the transmission time and communication resources have been updated. Taking link v as an example, the transition probability is E_v. Therefore, the channel link state remains unchanged, and the AoI at the RSU as well as the AoI on the link do not undergo any other change, continuing their linear growth. We have:
$$\boldsymbol{A'} = \boldsymbol{A} \cdot \boldsymbol{\psi_{l_3}} = [A_r, A_v], \bar{\boldsymbol{Q}}_{sl_3}{}' = \bar{\boldsymbol{Q}}_{sl_3} \cdot \boldsymbol{\psi_{l_3}} = [\bar{Q}_{00}, \bar{Q}_{01}].$$

Based on [39], we know that the link k's AoI is:
$$\bar{\Delta}_k = \sum \bar{Q}_{s0}, \quad \forall k \in 1, 2, \ldots, N_v. \tag{21}$$

According to Eq. (21), our next objective is to obtain $\bar{Q}_{s0}$. First, according to the theory in [40], we can obtain:
$$\bar{\boldsymbol{Q}}_{\boldsymbol{sl_a}}(\sum_{l_a} \eta_{l_a}) = \boldsymbol{b_s}\bar{\pi}_s + \sum_{l_2} \eta_{l_a} \bar{\boldsymbol{Q}}_{\boldsymbol{sl_b}} \boldsymbol{\psi_{l_b}}, l_a \in L_s, \; l_b \in L'_s, \tag{22}$$
where $\boldsymbol{b_s}$ is a binary differential vector coefficient used to characterize the AoI under state s, and $\bar{\pi}_s$ is the steady-state probability of state s. Furthermore, l_a and l_b denote the transitions between discrete state inputs and outputs, while L and L' represent the sets of inputs and outputs transitions.

Considering that the vehicle's data is generated only after it obtains communication resources, i.e., after it begin to transmit, the link k's AoI increases linearly with slope one only when $s = k$. However, the AoI at the RSU keeps increasing until it receives data from the link. Therefore, $\boldsymbol{b_s}$

can be expressed as:

$$\left.\begin{cases} \boldsymbol{b_s} = [1,0], for\ \forall s \neq k \\ \boldsymbol{b_s} = [1,1], for\ \forall s = k. \end{cases}\right\} \tag{23}$$

Next, we need to obtain $\bar{\pi}_s$. As stated by [40], the $\bar{\pi}_s$ satisfies the following conditions:

$$\bar{\pi}_s \sum_{l \in L_s} \eta_l = \sum_{l \in L'_s} \eta_l \bar{\pi}_{sl}, \sum_{s \in S} \bar{\pi}_s = 1,\ \mathrm{s} \in S. \tag{24}$$

Substituting η_l into Eq. (24), the $\bar{\pi}_s$ is shown as:

$$\begin{cases} \bar{\pi}_0 = \dfrac{1}{N_F} \\ \bar{\pi}_k = \dfrac{R_k}{N_F(H_k - E_k)}, \end{cases} \tag{25}$$

where N_F is a normalization factor, which is:

$$N_F = 1 + \sum_{k=1}^{N_v} \frac{R_k}{H_k - E_k}. \tag{26}$$

Next, when $s = 0$, according to the analysis in [30], we know that the left side of Eq. (22) represents the system state transitioning to busy—that is, transitioning to a state not equal to zero—while the right side represents the system state transitioning to idle, i.e., s transitions to 0. When $s = 0$, the channel is idle, so $\boldsymbol{b_s} = [1, 0]$. The transitions on the left side correspond to states from 1 to n and from $2n+1$ to $3n$, while the right side correspond to states from $n+1$ to $2n$.

Moreover, based on the analysis in [40], Eq. (22) applies to any reset mapping and therefore also applies to mappings caused by the re-evaluation mechanism. Substituting $s = 0$ into Eq. (22), we obtain:

$$\bar{Q}_{00}(\sum_{s=1}^{N_v} R_s) + \sum_{\substack{s=1 \\ s \neq k}}^{N_v} \bar{Q}_{s0} \cdot E_s = \bar{\pi}_0 + \sum_{\substack{s=1 \\ s \neq k}}^{N_v} H_s \bar{Q}_{s0} + H_k \bar{Q}_{k1}, \tag{27}$$

$$\bar{Q}_{01}(\sum_{s=1}^{N_v} R_s) + \sum_{\substack{s=1 \\ s \neq k}}^{N_v} \bar{Q}_{s1} \cdot E_s = \sum_{\substack{s=1 \\ s \neq k}}^{N_v} H_s \bar{Q}_{s1}. \tag{28}$$

Next, considering the case when $s \neq 0$, the left side of Eq. (22) represents the system state transitioning to idle, while the right side represents the system state transitioning to busy, i.e., transitioning to a state not equal to 0. The transitions on the left correspond to states from $n+1$ to $2n$, and those on the right denote states from 1 to n and from $2n+1$ to $3n$. Substituting $s \neq 0$ into Eq. (22), we obtain:

$$\bar{Q}_{s0} \cdot H_s = \bar{\pi}_s + R_s \cdot \bar{Q}_{00} + E_s \bar{Q}_{s0}, for\ \forall s = \{1, 2, ..., N_v\} \tag{29}$$

$$\bar{Q}_{s1} \cdot H_s = R_s \cdot \bar{Q}_{01} + \bar{Q}_{s1} E_s, for\ \mathrm{s} \neq k \tag{30}$$

$$\bar{Q}_{k1} \cdot H_k = \bar{\pi}_k + R_k \cdot \bar{Q}_{01} + \bar{Q}_{k1} E_k, for\ s = k. \tag{31}$$

Next, based on Eq. (27) to Eq. (31), we proceed to derive $\bar{Q}_{s0}$. First, according to Eq. 29, we have:

$$\bar{Q}_{s0} = \frac{\bar{\pi}_s + R_s \cdot \bar{Q}_{00}}{H_s - E_s}. \tag{32}$$

According to Eq. (32), it can be seen that the next step is to derive $\bar{Q}_{00}$. To obtain $\bar{Q}_{00}$, we note from Eq. (27) that it requires $\bar{Q}_{k1}$. We rearrange Eq. 30:

$$\bar{Q}_{s1} = \frac{R_s \cdot \bar{Q}_{01}}{H_s - E_s}. \tag{33}$$

We rearrange Eq. (31) as follows:

$$\bar{Q}_{k1} = \frac{\bar{\pi}_k + R_k \cdot \bar{Q}_{01}}{H_k - E_k}. \tag{34}$$

Substituting Eq. (33) into Eq. (28), we obtain:

$$\bar{Q}_{01} \cdot R_k \cdot (1 + \frac{E_k}{H_k - E_k}) = 0. \tag{35}$$

Since R_K, E_K, and H_K are all greater than zero, We get:

$$\bar{Q}_{01} = 0. \tag{36}$$

Therefore, substituting Eq. (36) into Eq. (34), we obtain:

$$\bar{Q}_{k1} = \frac{\bar{\pi}_k}{H_k - E_k}. \tag{37}$$

Finally, substituting Eq. (32) and Eq. (37) into Eq. (27), we obtain:

$$\bar{Q}_{00} = \frac{H_k - E_k}{H_k \cdot R_k}. \tag{38}$$

Then, according to Eq. (32), we obtain $\bar{Q}_{s0}$. In the end, we substitute Eq. (38) and Eq. (32) into Eq. (21), the AoI of link k can be expressed as:

$$\begin{aligned} \bar{\Delta}_k &= \sum_{s=0}^{N_v} \bar{Q}_{s0} \\ &= \frac{H_k - E_k}{H_k \cdot R_k}[1 + \sum_{s=1}^{N_v} \frac{R_s}{H_s - E_s}] + \sum_{s=1}^{N_v} \frac{\bar{\pi}_s}{H_s - E_s}. \end{aligned} \tag{39}$$

Subsequently, we get the mean AoI:

$$\bar{\Delta} = \frac{\sum_{k=1}^{N_v} \bar{\Delta}_k}{N_v}, \tag{40}$$

where $\bar{\Delta}$ denotes the network's averaged AoI.

Finally, we define the transfer probability under NR V2X Mode 2, namely H_v, R_v, and E_v. According to [30], the average service probability can be expressed as:

$$H_v = \frac{1}{T_v^H}, for\ \forall i \in \{1, 2, ...N_v\}, \tag{41}$$

where T_v^H represents the average time for successful transmission for vehicle v, which can be expressed as [41]:

$$T_v^H = t_p^v + t_{fa}^v + t_w^v + t_t^v, \tag{42}$$

where t_p^v is the data processing time, t_{fa}^v is the frame alignment duration, t_w^v the resource allocation period i.e., the

vehicle's selection window size, and t_t^v the data transmission time. Likewise, the average failure rate can be represented by:

$$R_v = \frac{1}{T_v^R}, for\ \forall i \in \{1, 2, ...N_v\}, \tag{43}$$

$$T_v^R = T_v^H + n \cdot T_r, \tag{44}$$

where T_r denotes the retransmission time after a failure. Based on the SHS model [40],we know that the transition rate is determined by the duration of the transition, thus, the re-evaluation mechanism transition probability is:

$$E_v = \frac{1}{T_v^E}, \tag{45}$$

where T_v^E denotes the average time of the re-evaluation, which is determined by the new selection window size of the re-evaluation mechanism. According to [13], [42], [43], the re-evaluation window is autonomously determined by the vehicle based on its specific SCI data.

VI. Optimization Objective and Solutions

In this section, we choose to solve the problem using the sequential convex approximation [44] and LLM-based MOEA/D algorithm (LLM-MO) [45]. We chose SCA because SCA can iteratively approximate the key non-convex terms and has theoretical convergence, interpretability, and high efficiency. In contrast, LLM-MO is designed for high-dimensional and highly nonlinear scenarios, and utilizes LLMs to generate high-quality solutions.

A. Optimization Objective

Based on section IV, we can define the fair access problem as a multi-objective optimization problem:

$$\begin{aligned} G_v(\boldsymbol{w}) &= \left| G_{fair}^v(\boldsymbol{w}) - G_{fair}(\boldsymbol{w}) \right|, \\ s.t\ \boldsymbol{w} &= \{w^1, w^2, \ldots, w_v^N\}, \\ v &\in \{1, 2, \ldots, N_v\}. \end{aligned} \tag{46}$$

Meanwhile, consider the AoI: $G_{N_v+1}(\boldsymbol{w}) = \min \bar{\Delta}$. Therefore, the overall optimization objective is given by:

$$\begin{aligned} \min_{\boldsymbol{w}}\ & \boldsymbol{G}(\boldsymbol{w}) = [G_1(\boldsymbol{w}), G_2(\boldsymbol{w}), \ldots, G_{N_v}(\boldsymbol{w}), G_{N_v+1}(\boldsymbol{w})]^T \\ & s.t\ C_1 : V_{\min} \le V_v \le V_{\max}, v \in [1, \ldots, N_v], \\ & \quad C_2 : w_{\min} \le w_v \le w_{\max}, v \in [1, \ldots, N_v]. \end{aligned} \tag{47}$$

According to the 3GPP standard [42], $w_{\min}$ and $w_{\max}$ denote the boundary limitation of windows.

B. SCA Algorithm

Since Eq. (47) is a multi-objective optimization problem, we first need to transform it into a single-objective problem. The problem contains several non-convex components, such as absolute value terms, PR_v and $H_v \cdot R_v$. To deal with this problem, we consider the auxiliary variables to replace the non-convex terms and use Taylor expansion to approximate the non-convex parts of the objective and constraints. The final problem is transformed into a convex problem, which is able to be efficiently addressed through classical convex optimization, including interior-point algorithms and Alternating Direction Method of Multipliers (ADMM) [46].

First, we use the weighted sum method [47] to convert the original optimization problem into a single-objective problem:

$$\begin{aligned} \min_{\boldsymbol{w}}\ & \boldsymbol{G}(\boldsymbol{w}) = \sum\nolimits_{v=1}^{N_v} \lambda_v \cdot G_v(\boldsymbol{w}) + \lambda_{N_v+1} \cdot G_{N_v+1}(\boldsymbol{w}), \\ & s.t\ C_1, C_2, \end{aligned} \tag{48}$$

where the $\lambda_v, v \in [1, \ldots, N_v + 1]$ is the weight used to keep the balance between different objectives. Since $\left| G_{fair}^v(\boldsymbol{w}) - G_{fair}(\boldsymbol{w}) \right|$ is a non-convex term, in order to remove the absolute value term, we introduce an auxiliary variable $z_v \ge 0$ which satisfies:

$$\begin{aligned} C_3 &: z_v \ge G_{fair}^v(\boldsymbol{w}) - G_{fair}(\boldsymbol{w}), \\ C_4 &: z_v \ge -(G_{fair}^v(\boldsymbol{w}) - G_{fair}(\boldsymbol{w})). \end{aligned} \tag{49}$$

Thus, Eq. (48) can be rewritten as:

$$\begin{aligned} \min_{\boldsymbol{w}}\ & \boldsymbol{G}(\boldsymbol{w}) = \sum\nolimits_{v=1}^{N_v} \lambda_v z_v + \lambda_{N_v+1} \cdot G_{N_v+1}(\boldsymbol{w}) \\ & s.t\ C_1, C_2, C_3, C_4. \end{aligned} \tag{50}$$

However, since there are still non-convex terms in $G_{fair}^v(\boldsymbol{w})$ and $G_{N_v+1}(\boldsymbol{w})$, Eq. (50) remains a non-convex function, we choose to apply the Sequential Convex Approximation (SCA) method to handle the non-convex terms. First, we tansfer $G_{fair}^v(\boldsymbol{w})$ into convex. Since the non-convex terms in $G_{fair}^v(\boldsymbol{w})$ is PR_v which involves extensive products, it will leads to an increase in complexity. So we apply the logarithm to transform the product terms into a summation form:

$$\log PR_v = \sum_{j \ne v} \log\left(1 - \delta_{v,j}(w)\right). \tag{51}$$

Note that the problem is still non-convex because $\delta_{v,j}$ is non-convex, and $\log(1-x)$ is a concave function. For each term, we perform SCA at the current t-th iteration point $\delta_{v,j}^{(t)}$. By applying a Taylor expansion to each term, we get:

$$\log(1-\delta_{v,j}(w)) = \log(1-\delta_{v,j}^{(t)}) - \frac{1}{1-\delta_{v,j}^{(t)}} \cdot \left(\delta_{v,j}(w) - \delta_{v,j}^{(t)}\right). \tag{52}$$

Substituting this into the previous expression, we obtain:

$$\log PR_v = C_v^{(t)} - \sum_{j \ne v} \frac{1}{1-\delta_{v,j}^{(t)}} \cdot \left(\delta_{v,j}(w) - \delta_{v,j}^{(t)}\right), \tag{53}$$

where $C_v^{(t)} = \sum\limits_{j \ne v} \log(1 - \delta_{v,j}^{(t)})$ is a constant. We continue by substituting the explicit form of $\delta_{v,j}(w)$ into the above approximated expression, resulting in a convex approximation formula that is more suitable for numerical solving. We then perform a first-order Taylor expansion on $\delta_{v,j}(w)$:

$$\delta_{v,j}(w) = \delta_{v,j}(w^{(t)}) + \nabla_w \delta_{v,j}(w^{(t)})^\top (w - w^{(t)}). \tag{54}$$

We combine the terms that are not optimization variables into c. Since $\delta_{v,j}(w)$ is a function of w_v and w_j, we take the partial

derivatives with respect to w_v and w_j, yielding:

$$\frac{\partial \delta_{v,j}}{\partial w_v} = \frac{\partial}{\partial w_v}\left(\frac{[(w_v+1)(w_j+1)]^2}{c(w_v+w_j+1)}\right), \tag{55}$$

which can be numerically computed in each iteration. We now summarize the previous results as follows:

$$\log PR_v(w) = \sum_{j\neq v}\log(1-\delta_{v,j}^{(t)}) \ -\sum_{j\neq v}\frac{1}{1-\delta_{v,j}^{(t)}}\cdot \\ \left[\nabla_{w_v}\delta_{v,j}^{(t)}(w_v-w_v^{(t)})+\nabla_{w_j}\delta_{v,j}^{(t)}(w_j-w_j^{(t)})\right]. \tag{56}$$

After organizing, we obtain:

$$\log PR_v = C_v^{(t)}+\sum_{j\neq v}a_{v,j}^{(t)}(w_v-w_v^{(t)})+b_{v,j}^{(t)}(w_j-w_j^{(t)}). \tag{57}$$

where

$$a_{v,j}^{(t)} = -\frac{1}{1-\delta_{v,j}^{(t)}}\cdot\frac{\partial\delta_{v,j}}{\partial w_v}\bigg|_{w^{(t)}} \ b_{v,j}^{(t)} = -\frac{1}{1-\delta_{v,j}^{(t)}}\cdot\frac{\partial\delta_{v,j}}{\partial w_j}\bigg|_{w^{(t)}} \tag{58}$$

We have transformed $G_{fair}^v(\boldsymbol{w})$ into a convex function:

$$G_{fair}^v(\boldsymbol{w}) = \frac{\sum_{k=1}^{k=G}\xi(S_{vk},G_{vk})\cdot\log_2(1+\frac{p_v\cdot h_v\cdot {d_v}^{-\partial}}{\sigma^2})}{V_v}\cdot \\ \exp(-(C_v^{(t)}+\sum_{j\neq v}(a_{v,j}^{(t)}(w_v-w_v^{(t)})+b_{v,j}^{(t)}(w_j-w_j^{(t)})))). \tag{59}$$

Next, we consider $\bar{\Delta}(w)$. We divide $\bar{\Delta}_k$ into two parts:

$$A(w_k) = \frac{H_k-E_k}{H_k\cdot R_k}[1+\sum_{s=1}^{N_v}\frac{R_s}{H_s-E_s}] \\ = \left(w_k+c_2^k\right)\left[1-c_3^k(w_k+c_1^k)\right]\cdot \\ \left(1+\sum_{s=1}^{N_v}\frac{w_s+c_1}{(w_s+c_2^s)\left[1-c_3^s(w_s+c_1^s)\right]}\right) \tag{60}$$

$$B(\boldsymbol{w}) = \sum_{s=1}^{N_v}\frac{\bar{\pi}_s}{H_s-E_s}, \tag{61}$$

where c_1^k, c_2^k and c_3^k respectively denote the terms independent of w in H_k, R_k and E_k. We proceed with a Taylor expansion, which first requires taking derivatives. To facilitate differentiation, we have: $A(w_k) = A_1(w_k)\cdot A_2(w_k)$, where:

$$A_1(w) = \left(w_k+c_2^k\right)\left[1-c_3^k(w_k+c_1^k)\right]. \\ A_2(w) = \left(1+\sum_{s=1}^{N_v}\frac{w_s+c_1^s}{(w_s+c_2^s)\left[1-c_3^s(w_s+c_1^s)\right]}\right). \tag{62}$$

Therefore, we have:

$$\frac{\partial A(w_k)}{\partial w_k} = \frac{dA_1(w_k)}{dw_k}\cdot A_2(w_k)+A_1(w_k)\cdot\frac{dA_2(w_k)}{dw_k}. \tag{63}$$

According to the first-order Taylor expansion, we have:

$$A(w_k) = A({w_k}^{(t)})+A'({w_k}^{(t)})(w-w_k^{(t)}). \tag{64}$$

Algorithm 1: SCA Iteration Algorithm

Input: speed V, vehicle numbers N_v, tolerance ε, maximum iteration G_{max}, learning rate β.
Output: $\boldsymbol{w}^*$

Initialization Phase:
Set iteration index $t=0$
Initialize variables $\boldsymbol{w}^{(0)}$
Set convergence tolerance ε and G_{max}
Main Iteration:
while $\|\boldsymbol{w}^{(t+1)}-\boldsymbol{w}^{(t)}\|\leq\varepsilon$ *and* $t<G$ **do**
  Step 1: Formulate the single-objective optimization problem based on Eq. 48.
  Step 2: Introduce auxiliary variables to construct Eq. 50.
  Step 3: Convexify $G_{fair}^v(\boldsymbol{w})$ with Eq. 51-59.
  Step 4: Convexify $G_{N_v+1}(\boldsymbol{w})$ with Eq. 60-67.
  Step 5: Formulate the current optimization problem 68 based on the current solution $\boldsymbol{w}^{(t)}$.
  Step 6: Apply ADMM to solve 68 to get $\boldsymbol{w}^{(t+1)}$.
  Step 7: Update $\boldsymbol{w}^{(t+1)} = \beta\cdot\boldsymbol{w}^{(t+1)}+(1-\beta)\cdot\boldsymbol{w}^{(t)}$.
  Step 8: Check for convergence: **if** $\|\boldsymbol{w}^{(k+1)}-\boldsymbol{w}^{(t)}\|\leq\varepsilon$ **then**
    Exit the loop.
  Increment t
return $\boldsymbol{w}^*=\boldsymbol{w}^{(t+1)}$

Next, we apply the same method to process $B(\boldsymbol{w})$:

$$B(\boldsymbol{w}) = \sum_s\left[B(w_s^{(t)})+\nabla B(w_s^{(t)})(w_s-w_s^{(t)})\right]. \tag{65}$$

Thus, convex approximation of $\bar{\Delta}_k$ can be expressed as:

$$\bar{\Delta}_k = A(w_k)+B(\boldsymbol{w}). \tag{66}$$

The AoI is given by:

$$\bar{\Delta}(\boldsymbol{w}) = \frac{\sum_{k=1}^{N_v}\bar{\Delta}_k}{N_v}. \tag{67}$$

Now, we have transformed the non-convex terms in the optimization objective into convex functions. Therefore, the optimization objective is given by:

$$\min_{\boldsymbol{w}} \ \boldsymbol{G}(\boldsymbol{w}) = \sum\nolimits_{v=1}^{N_v}\lambda_v z_v+\lambda_{N_v+1}\bar{\Delta}(\boldsymbol{w}) \\ s.t\ C_1, C_2, C_3, C_4. \tag{68}$$

Next, we can adopt convex optimization methods to solve this problem. In each SCA iteration, a new optimization problem is formulated and solved using ADMM to obtain the current solution $\boldsymbol{w^t}$. To prevent the $\boldsymbol{w}^{(t+1)}$ from spanning too widely compared with $\boldsymbol{w}^{(t)}$, we introduce β as the learning rate to limit the update speed of $\boldsymbol{w}^{(t+1)}$. The iteration proceeds until either convergence or G_{max} is achieved. The algorithm framework is shown in Algorithm 1.

C. LLM-MO Algorithm

The proposed LLM-MO algorithm builds upon the traditional MOEA/D framework [45], with the key novelty being the integration of an LLM-guided crossover mechanism. The overall process can be divided into three main stages: initialization, iteration, and solution update. In the LLM-MO algorithm, the weight vectors $\boldsymbol{m} = \{\mathbf{m}_1, \ldots, \mathbf{m}_H\}$ are initially created using the Das-Dennis uniform sampling scheme. This procedure decomposes the multi-objective problem into H distinct subproblems, each corresponding to a specific optimization direction. To identify the T nearest neighbors of each weight vector, the cosine similarity is computed as:

$$\cos(\mathbf{m_i}, \mathbf{m_j}) = \frac{\mathbf{m_i} \cdot \mathbf{m_j}}{|\mathbf{m_i}||\mathbf{m_j}|}. \tag{69}$$

Population initialization is then performed by assigning random initial solutions to each weight vector. The ideal point is initialized to record the current optimal values for each objective, which will guide subsequent optimization directions (This concludes Steps 1-6 of the algorithm.).

In each iteration cycle: For every subproblem, parent solutions are selected using a probability p_{near}, which is determined based on the neighborhood relationships; if no neighborhood relationship is established, random selection is used. Afterward, LLM-guided crossover operations are performed. In this process, the LLM functions as a black-box operator that generates a new set of offspring solutions based on the parent solutions and their corresponding objective values.

To manage the complexity of the LLM inputs and reduce the impact of numerical range issues on inference stability, the input data is normalized. The inputs consist of the set of parent solutions from the previous step and their associated objective values, represented as w and $G(w)$.

Next, the prompt for the LLM is structured through prompt engineering. The prompt is broken down into three key sections:

1. A thorough description of the task; 2. The input data to be processed; 3. The expected format for the output data.

For the specific optimization task described in this paper, the prompt is formulated as follows: "You are tasked with optimizing a multi-objective optimization problem. I will provide you with multiple optimization variables and their corresponding objective values. Based on these inputs, generate new offspring solutions, ensuring that the objective values of the offspring are at least as good as or better than the parent solutions."

Following this, the input data is provided as $[w_1, w_2, ...w_H]$, along with $[G(w_1), G(w_2), ...G(w_H)]$. The output should include only the offspring solutions, where each offspring solution starts with <start> and ends with <end>. No further explanations should be included.

Once the prompt is complete, the LLM, as a black-box operator, can generate a fresh set of offspring solutions.

> You will perform a multi-objective optimization task. I will provide you with multiple sets of data, where each set includes window size and their corresponding fairness index differences and AoI. Each set starts with <begin> and finishes with <end>.
> point: <begin>0.124,0.352,0.421 <end>
> value: <begin>0.021,0.031,0.012,67 <end>
> Based on these data, provide one set of window sizes different from the above data, whose objective values are better than the given data. Your answer should start with <begin> and finish with <end>.

Denormalized solutions update the ideal point and optimize neighboring subproblems, the h th Subproblem can be formulated as:

$$g(\boldsymbol{w} \mid \boldsymbol{m}_h, \boldsymbol{z^*}) = \max_{1 \le n \le N_v+1} \{\boldsymbol{m}_h \,|\, G_n(\boldsymbol{w}) - z_n^*|\}, \tag{70}$$

where z^* denotes the ideal point, $\mathbf{m_h}$ is the h th weight. Neighborhood solutions are replaced if offspring solutions exhibit superior performance on corresponding subproblems.(Steps 7 to 17 in algorithm 2.)

The Pareto solution set $\mathcal{P} = \{\boldsymbol{w_1}, \ldots, \boldsymbol{w_H}\}$ is obtained upon reaching maximum iterations. Optimal solution $w*$ is selected through:

(1) Filtering solutions with all objective values below predefined thresholds K_{bound};
(2) Selecting the solution with minimal G_{N_v+1} from threshold-satisfying candidates.

To adaptively determine K_{bound}, we first sort all fairness deviations in ascending order, and then select the minimal deviation among the largest 10% of them. Thus, K_{bound} can be described as:

$$K_{bound} = \min \left\{ G_v(\boldsymbol{w})^{(j)} \;\middle|\; j = \lceil 0.9\mathcal{P} \rceil, \ldots, \mathcal{P} \right\}, \tag{71}$$

where $G_v(\boldsymbol{w})^{(j)}$ represents the j-th smallest value in the ascendingly ordered sequence of all fairness deviations $G_v(\boldsymbol{w})$.

Now, we obtain the optimal selection window size $w*$.(Steps 18 to 23 in algorithm 2.)

D. Computational Complexity Analysis

In this section, we will analyze the computational complexity of our approaches.

First, we analyze the computational complexity of the SCA algorithm. SCA typically consists of two main time-consuming parts: the convexification operation in each iteration and the iterative solution of the convex optimization subproblem using ADMM. Therefore, its overall complexity can be written as: $O(G_{max} \cdot (C_{\text{convex}} + C_{\text{ADMM}}))$, where G_{max} is the maximum number of outer-loop iterations for SCA , C_{convex} is the complexity required for linearization each time, and C_{ADMM} is the complexity of solving the convex optimization each time.

The main source of complexity in the convexification operation comes from gradient operations. For convexifying G_{fair}, considering that each vehicle v couples with all other vehicles j, it is necessary to compute gradients for all vehicles,

Algorithm 2: LLM-MO: LLM-guided MOEA/D

Input: Number of objectives $N_v + 1$, number of subproblems H, neighborhood size T, neighborhood selection probability P_{near}, maximum iterations N_{iter}, vehicle speed V

Output: $\boldsymbol{w}^*$

1 Define weight $\{\boldsymbol{m}^1, \ldots, \boldsymbol{m}^H\}$ by Das-Dennis sampling
2 **for** *each subproblem* $h \in \{1, \ldots, H\}$ **do**
3 Define neighborhood B^h with T nearest weight
4 Randomly initialize population $\mathcal{P} = \{\boldsymbol{w}^1, \ldots, \boldsymbol{w}^H\}$
5 Evaluate $\boldsymbol{G}(\boldsymbol{w}^i) = (G_1, \ldots, G_{N_v+1})$ for all $i \in H$
6 Initialize ideal point $z^* = \{\min G_1, \ldots, \min G_{N_v+1}\}$
7 **for** $iter \leftarrow 1$ **to** N_{iter} **do**
8 **for** $h \leftarrow 1$ **to** H **do**
9 With probability P_{near} select parents from B^h; otherwise select from $\mathcal{P}$
10 Construct LLM prompt with parents
11 Query LLM to generate offspring $\boldsymbol{w_{new}}$
12 Evaluate offspring $\boldsymbol{G(w_{new})}$
13 Update ideal point: $\boldsymbol{z^*} \leftarrow \min\left(\boldsymbol{z^*}, \boldsymbol{G(w_{new})}\right)$
14 Define the subproblem as: $g(\boldsymbol{w} \mid \boldsymbol{m}_h, \boldsymbol{z^*}) = \max_{1 \le n \le N_v+1} \{\boldsymbol{m}_h \,|\, G_n(\boldsymbol{w}) - z_n^*|\}$
15 **for** *each* $j \in B^h$*:* **do**
16 **if** $g(\boldsymbol{w_{new}} \mid \boldsymbol{m}^j, \boldsymbol{z^*}) \le g(\boldsymbol{w}^j \mid \boldsymbol{m}^j, \boldsymbol{z^*})$ **then**
17 $\boldsymbol{w}^j \leftarrow \boldsymbol{w_{new}}$
18 Set $\bar{\Delta}(\boldsymbol{w}) = +\infty$
19 **foreach** $p \in \mathcal{P}$ **do**
20 **if** $G_i \le K_{bound}, i \in p$ **then**
21 **if** $G_{N_v+1} \le age$ **then**
22 $\bar{\Delta}(\boldsymbol{w}) \leftarrow G_{N_v+1}$
23 $\boldsymbol{w}^* \leftarrow \boldsymbol{w}^p$
24 **return** $\boldsymbol{w}^*$

i.e., $O(N_v^2)$. Additionally, considering the gradient operations when convexifying AoI, since $B(\boldsymbol{w})$ is a summation term over all vehicles and π_s also involves summation over all vehicles, the convexification complexity of $B(\boldsymbol{w})$ also includes $O(N_v^2)$. However, due to the presence of π_s, the complexity of $B(\boldsymbol{w})$ is $O(N_v^2) + O(N_v)$. Therefore, ignoring constant terms, the total convexification complexity is $O(N_v^2) + O(N_v)$.

Next, we analyze the complexity of solving the convex problem using ADMM. Since auxiliary variables are introduced, the convex problem to be solved contains $2N_v$ optimization variables, requiring the solution of an $N_v \times N_v$ system of linear equations, resulting in a computational complexity of $O(N_v^3)$. Additionally, considering that updating Lagrange multipliers is involved, there is also an $O(N_v)$ computational cost. Hence, the complexity of solving the convex problem is $O(N_v^3) + O(N_v)$. Let the number of ADMM iterations be T_{ADMM}, then the complexity of each ADMM solution is $T_{\text{ADMM}} \cdot (O(N_v^3) + O(N_v))$. Therefore, the total computational complexity of SCA is expressed as: $O\left(G_{\max} \cdot \left(O(N_v^2) + O(N_v) + T_{\text{ADMM}} \cdot (O(N_v^3) + O(N_v))\right)\right)$. Considering the magnitude of $G_{\max}$ and T_{ADMM}, the $O(N_v)$ terms can be neglected. Thus, the overall complexity can be expressed as: $O\left(G_{max} \cdot \left(O(N_v^2) + T_{\text{ADMM}} \cdot O(N_v^3)\right)\right)$.

Next, we analyze the computational complexity of the LLM-MO algorithm. The complexity analysis can be divided into two parts: the initialization phase and the iterative phase. Since the initialization phase is executed only once, its complexity is much smaller than that of the iterative phase.

First, analyzing the initialization phase: generating H weight vectors, the complexity can be expressed as $O(H)$. Next, constructing neighborhoods: For each weight vector, compute cosine similarity with all others and retrieve top T, the cosine similarity complexity is $O(H)$, and the top T sorting is with $O(H \log T)$. Therefore, the total complexity at this point can be expressed as: $O(H(H + H \log T)) = O(H^2 + H^2 \log T)$.

Next, generating the initial solution set is with $O(H)$, computing the minimum value of each objective function over H solutions is with $O(H \cdot (N_v + 1))$. Therefore, the total complexity of the initialization phase can be expressed as: $O(H^2 \log T + H(N_v + 1))$.

Then entering the iterative phase: first the outer loop with G_{max} generations, followed by the inner loop with H subproblems. For each subproblem, randomly selecting neighbors or global individuals is with $O(T)$, normalizing input for $P_{parents}$ (assumed size M), constructing prompts is with $O(M)$. Calling the LLM for inference: assumed to be $O(C_{LLM})$. At most 3 attempts, so the total complexity at this step is: $O(M + C_{LLM})$. Next, updating the reference point: $O(N_v + 1)$, iterating over K neighbors: $O(T)$, computing $g(\mathbf{o}|\mathbf{w}_j, \mathbf{z}^*)$ each time is with $O(1)$. Therefore, the per-subproblem complexity per generation is given by: $O(T) + O(M + C_{LLM}) + O(N_v + 1) + O(T) = O(M + C_{LLM} + T + N_v)$.

Per-generation complexity (H subproblems): $H \cdot O(M + C_{LLM} + T + N_v)$. Complexity over N_{iter} generations: $GmaxH \cdot O(M + C_{LLM} + T + N_v)$. Finally, archive updating (lines 20–24): iterating over H individuals: $O(H)$.

So far, the initialization Phase complexity can be described as: $O(H^2 \log T + H(N_v + 1))$. The main Optimization Loop complexity can be described as: $O(G_{max}H(M + C_{LLM} + T + N_v)$. However, in practice, since the number of iterations N_{iter} is large, the computational complexity of the initialization phase can be ignored. Therefore, the overall algorithm complexity can be expressed as: $O(N_{\text{iter}}H(M + C_{LLM} + T + N_v)$.

VII. Numerical Simulation Result And Analysis

We will next demonstrate the reliability of the proposed scheme through numerical simulations. The benchmark algorithms for this experiment are several multi-objective algorithms. Our baseline algorithms include NSGA-II, SPEA2, NSGA-III, MOEA/D, MOPSP, and PPO-MO [48]. The baseline multi-objective algorithms are realized via the pymoo framework [49]. Meanwhile, this paper uses the QSOP solver in the cvxpy framework for convex optimization, which adopts

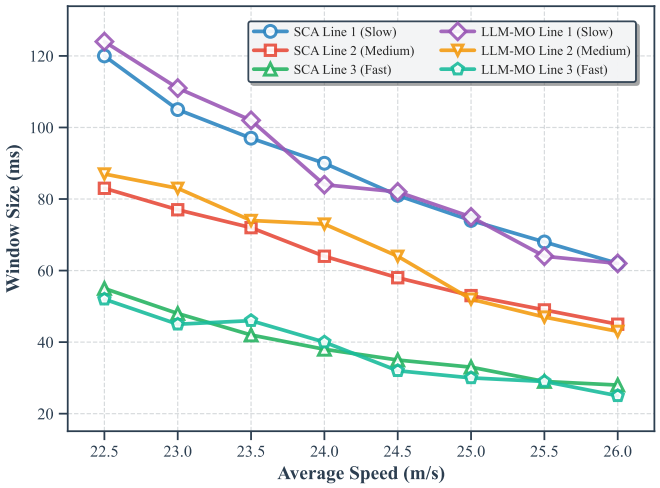

Fig. 4: Different Lines' Optimal Selection Window

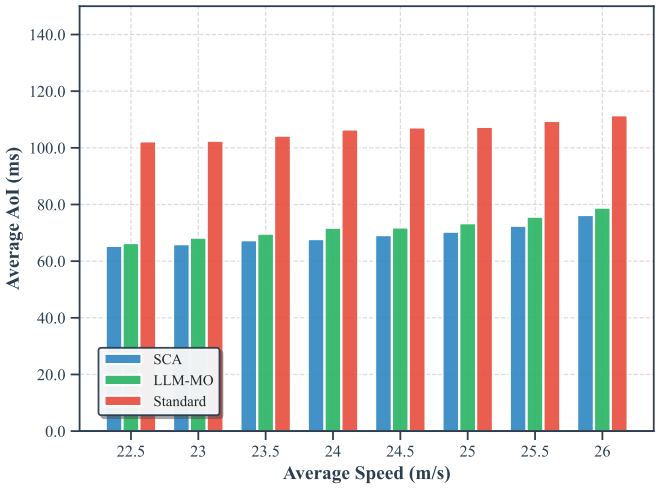

Fig. 6: Optimal AoI Comparison

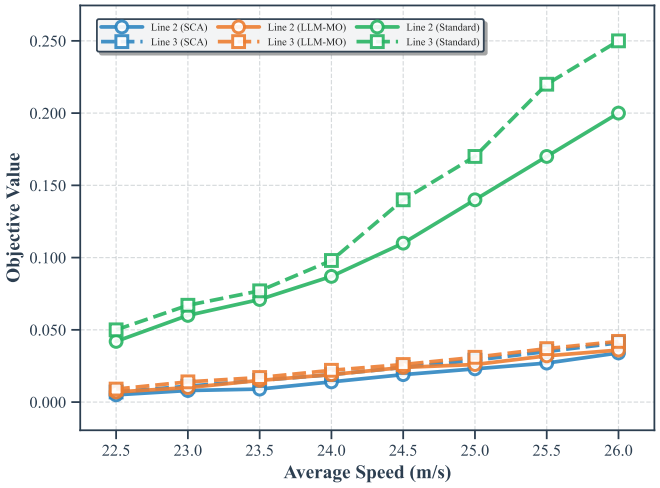

Fig. 5: Different Lines' Objective Value Comparison

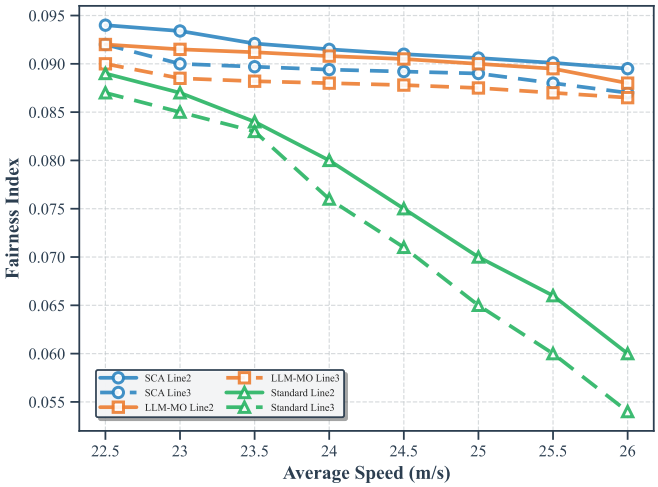

Fig. 7: Different Lines' Fairness index Comparison

ADMM [50]. In order to eliminate the randomness brought by a single experiment, the experimental data in this part have all been averaged over 20 or more times. Some important experimental parameters are shown in Table III.

Fig. 4 shows the trend of the selected window size with respect to the average vehicle speed after adopting the two schemes. With a rise in average vehicle speed, we can find that the window size for vehicles on the three lanes decreases, indicating that two schemes adapt the window size based on speed, thus accelerating the vehicle communication speed to reduce AoI. Additionally, we can observe that vehicles with slower speeds have larger window sizes, which reveals that two schemes can modify the window size depending on the vehicle's velocity, allowing faster vehicles to exchange more information and thus achieve fair access. Meanwhile, we also observe that when the vehicle speed is 24 m/s, the selection window would slightly increase. This is because at 24 m/s, there is a conflict point between AoI and fairness optimization, which led to a slight increase in the window size, which could significantly reduce AOI. Therefore, the optimizer is more inclined to slightly increase the window size at this point to achieve greater benefits.

Fig. 5 displays the fairness deviation for the first N objectives. We can see that vehicles using the two schemes have much smaller fairness differences than those using conventional protocols. This is because the two schemes can effectively tune the window size in order to ensure fair

TABLE III: Important parameters

Parameters	Value	Parameters	Value
R	$200m$	G_{max}	5000
B	$20MHZ$	α	3
w_{min}	$20ms$	w_{max}	$150ms$
β	0.2	RRI	$100ms$
N_v	3	σ^2	$9dB$
ε	0.01	t_{fa}	$0.468ms$
V_{min}	$20m/s$	V_{max}	$30m/s$
H	120	T	20
P_{near}	0.85	N_{iter}	1000

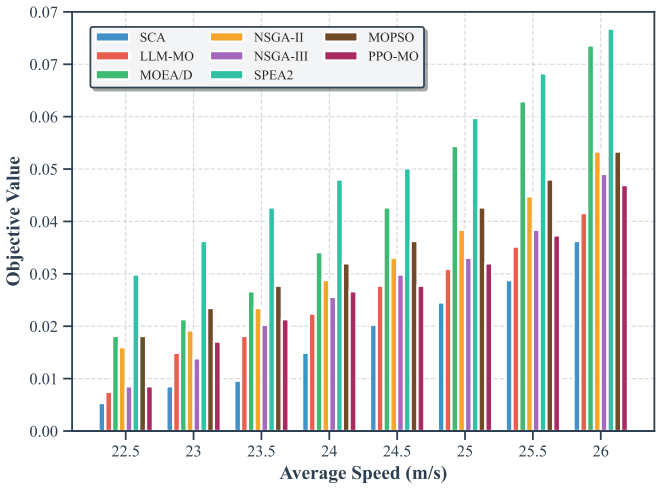

Fig. 8: Different algorithms' Objective Value Comparison

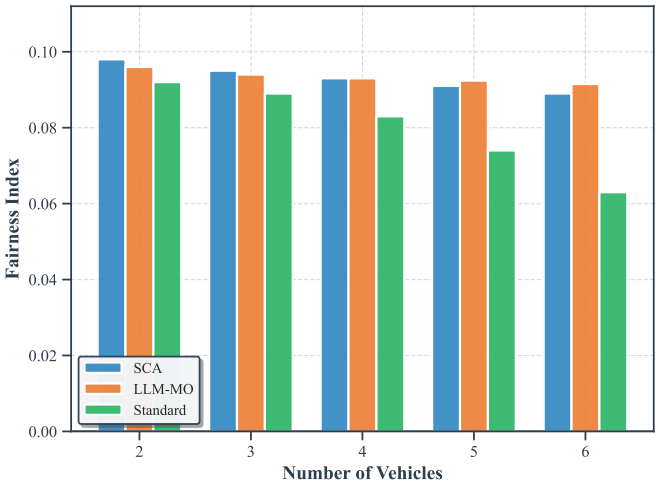

Fig. 10: Fairness Index Under Pressure Test

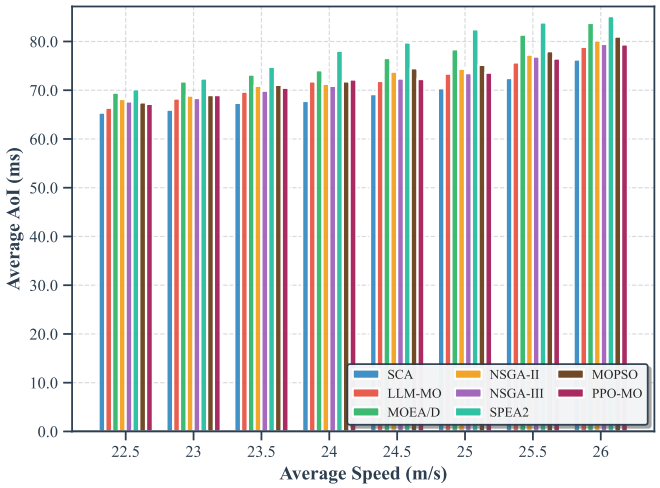

Fig. 9: Different algorithms' AoI comparison

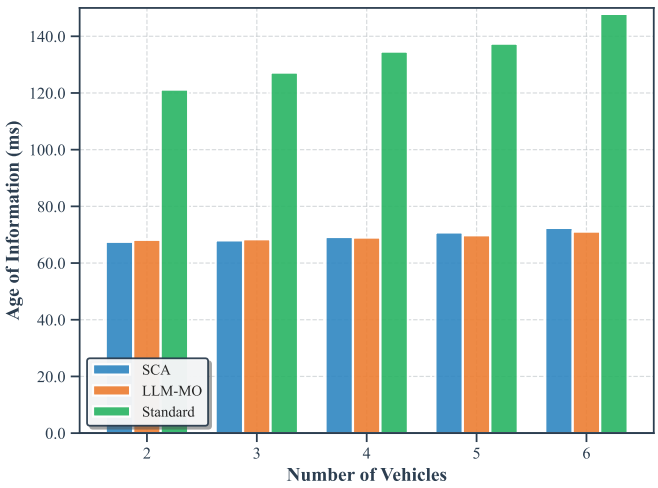

Fig. 11: AoI Under Pressure Test

access. Additionally, with a rise in average velocity, both two schemes' objective values increase. This can be attributed to the fact that faster velocity make fair access more challenging, and it becomes harder to balance the optimization of AoI, leading to a slight increase in fairness deviation. Notably, the second lane have slightly lower fairness deviations, as their speeds tend to be more average, resulting in smaller deviations compared to the overall network. Meanwhile, the performance of the LLM-MO algorithm is slightly inferior to that of the SCA algorithm, since LLMs struggle to conduct precise modeling and rely mainly on experience-driven reasoning.

Fig. 6 shows the trend of AoI as the vehicle speed changes. It can be seen that as the speed increases, the AoI for both schemes rises. This is due to the compromises made to achieve both fair access and AoI optimization. However, the AoI under the two schemes are significantly lower than that under conventional protocols, as the two schemes take into account the AoI optimization strategy under re-evaluation mechanism, adjusting window size according to the speed to minimize AoI.

From Fig. 4 to 7, it can be observed that different speeds have a significant impact on both fairness and AoI. As the speed gradually increases, we can conclude that when vehicle speed rises, our scheme typically reduces the selection window size to shorten communication time, thereby enabling high-speed vehicles to effectively acquire sufficient useful information and achieve fair access. Meanwhile, while maintaining a relatively stable fairness index, the scheme also keeps AoI consistently at a low level. This effectively demonstrates that our approach can adaptively adjust the selection window under different speed conditions, thereby jointly optimizing fairness and AoI.

The impact of vehicle speed on the fairness index is depicted in Fig. 7. As the average speed increases, the fairness index decreases for both schemes. This is due to the difficulty of optimizing both fair access and AoI when the speed increases. However, we observe that the fairness index for the two schemes remains relatively stable, while the index for the conventional protocol decreases significantly. This indicates that the proposed approach ensures fair access by appropriately tuning the selection window.

Fig. 8 shows the trend of the first N_v objective values under various benchmark algorithms with an increase in the averaged vehicle velocity. It can be observed that as the vehicle velocity grows, all algorithms exhibit an upward trend in objective values. However, the increase in objective values of the two proposed schemes is smaller than that of the benchmark algorithms, including NSGA-II, SPEA2, MOEA/D, and PPO-MO. This is because the SCA-based scheme performs convexification and solves a convex optimization problem, enabling more accurate solutions, while the LLM-MO scheme can generate better offspring solutions through LLM guidance. In contrast, benchmark algorithms require more iterations to obtain approximate solutions and PPO-MO is prone to getting stuck in local optima due to the influence of its reward function.

Fig. 9 shows the trend of AoI for different benchmark algorithms with a rise in the averaged vehicle velocity. We can find that with a rise in the averaged vehicle velocity, all the AoI slightly increases due to the difficulty of achieving fair access at higher speeds. However, the two schemes exhibit the lower AoI and the slower growth, as convex optimization can precisely find a solution that balances fair access and AoI and the LLM can obtain better offsprings.The performance of PPO-MO is slightly superior to that of other baseline algorithms, but it is still limited by its local optimum.

Fig. 10 and Fig. 11 show the performance of the two schemes under high-pressure. Fig. 10 presents the change in the fairness index for different vehicle numbers. We can see that a rise in vehicle number does have a slight impact on the fairness index, as the probability of conflict increases with more vehicles. However, the fairness index under conventional protocols decreases much more sharply. The influence of the number of vehicles on AoI is depicted in Fig. 11. We can see that the increase in vehicle numbers does not significantly affect AoI. The slight increase is due to delays caused by conflicts, indicating that the two schemes exhibit stable performance under high-pressure. Meanwhile, we can find that under high-pressure scenarios, LLM-MO behaves better than SCA. The reason is that under high-dimensional scenarios, the convexification of SCA introduces larger errors, whereas LLM generates offspring through experience-driven reasoning, making it less affected by dimensionality.

VIII. Conclusion

In this paper, we consider the problem of fair access. Based on an image semantic communication system, we define a fairness index to measure the extent to which vehicles achieve fair access and implement fair access by adjusting the selection window size. Additionally, we take the new re-evaluation mechanism into consideration. We model AoI using SHS and formulate a multi-objective optimization problem. According to the simulation, we conclude the following findings:

1) Vehicles with both high and low speeds exhibit large fairness differences, while vehicles with moderate speeds generally show better fair access performance. This is because their fairness index has a smaller difference from the average fairness index due to the moderate speed.
2) Considering that both the fairness index and AoI are functions of the selection window size and are related to the selection window of each vehicle, an inherent trade-off emerges: optimizing either one independently will lead to fluctuations in the other. Furthermore, as vehicle speed increases, the growing disparity in speeds makes achieving fair access more challenging than optimizing AoI. Consequently, under higher-speed conditions, the optimal solution tends to slightly favor fairness, leading to a minor increase in AoI. The joint optimization framework proposed in this paper achieves a balance between the two by simultaneously optimizing fairness and AoI, thereby avoiding extreme degradation in either metric and enabling a balanced improvement in overall performance.
3) Compared to existing multi-objective algorithms, both SCA and LLM-MO demonstrate higher accuracy and stability. SCA provides high-precision solutions through convex approximation, while LLM-MO exhibits greater robustness in complex or high-pressure scenarios due to its large model-guided offspring generation.

In future work, we might explore the problem of fair access in urban scenarios.

References

[1] X. Zhang, J. Li, J. Zhou, S. Zhang, J. Wang, Y. Yuan, J. Liu, and J. Li, "Vehicle-to-everything communication in intelligent connected vehicles: A survey and taxonomy," *Automotive Innovation*, pp. 1–33, 2025.

[2] X. Gu, Q. Wu, P. Fan, N. Cheng, W. Chen, and K. B. Letaief, "Drl-based federated self-supervised learning for task offloading and resource allocation in isac-enabled vehicle edge computing," *Digital Communications and Networks*, vol. 11, no. 5, pp. 1614–1627, 2025. [Online]. Available: https://www.sciencedirect.com/science/article/pii/S2352864824001755

[3] S. Feng, X. Yan, H. Sun, Y. Feng, and H. X. Liu, "Intelligent driving intelligence test for autonomous vehicles with naturalistic and adversarial environment," *Nature communications*, vol. 12, no. 1, p. 748, 2021.

[4] C. Ma, J. Zhu, M. Liu, H. Zhao, N. Liu, and X. Zou, "Parking edge computing: Parked-vehicle-assisted task offloading for urban vanets," *IEEE Internet of Things Journal*, vol. 8, no. 11, pp. 9344–9358, 2021.

[5] Z. Shao, Q. Wu, P. Fan, N. Cheng, W. Chen, J. Wang, and K. Ben Letaief, "Semantic-aware spectrum sharing in internet of vehicles based on deep reinforcement learning," *IEEE Internet of Things Journal*, vol. 11, no. 23, pp. 38 521–38 536, 2024.

[6] H. Yang, Z. Wei, Z. Feng, X. Chen, Y. Li, and P. Zhang, "Intelligent computation offloading for mec-based cooperative vehicle infrastructure system: A deep reinforcement learning approach," *IEEE Transactions on Vehicular Technology*, vol. 71, no. 7, pp. 7665–7679, 2022.

[7] I. Soto, M. Calderon, O. Amador, and M. Urueña, "A survey on road safety and traffic efficiency vehicular applications based on c-v2x technologies," *Vehicular Communications*, vol. 33, p. 100428, 2022.

[8] X. Wang, K. Tao, N. Cheng, Z. Yin, Z. Li, Y. Zhang, and X. Shen, "Radiodiff: An effective generative diffusion model for sampling-free dynamic radio map construction," *IEEE Transactions on Cognitive Communications and Networking*, vol. 11, no. 2, pp. 738–750, 2025.

[9] J. Wang, W. Chai, A. Venkatachalapathy, K. L. Tan, A. Haghighat, S. Velipasalar, Y. Adu-Gyamfi, and A. Sharma, "A survey on driver behavior analysis from in-vehicle cameras," *IEEE Transactions on Intelligent Transportation Systems*, vol. 23, no. 8, pp. 10 186–10 209, 2021.

[10] X. Luo, H.-H. Chen, and Q. Guo, "Semantic communications: Overview, open issues, and future research directions," *IEEE Wireless communications*, vol. 29, no. 1, pp. 210–219, 2022.

[11] Z. Zhang, Q. Wu, P. Fan, N. Cheng, W. Chen, and K. B. Letaief, "Drl-based optimization for aoi and energy consumption in c-v2x enabled iov," *IEEE Transactions on Green Communications and Networking*, vol. 9, no. 4, pp. 2144–2159, 2025.

[12] Y. Shao, Q. Cao, and D. Gündüz, "A theory of semantic communication," *IEEE Transactions on Mobile Computing*, vol. 23, no. 12, pp. 12 211–12 228, 2024.

[13] M. H. C. Garcia, A. Molina-Galan, M. Boban, J. Gozalvez, B. Coll-Perales, T. Şahin, and A. Kousaridas, "A tutorial on 5G NR V2X communications," *IEEE Communications Surveys & Tutorials*, vol. 23, no. 3, pp. 1972–2026, 2021.

[14] M. M. Saad, M. T. R. Khan, S. H. A. Shah, and D. Kim, "Advancements in vehicular communication technologies: C-v2x and nr-v2x comparison," *IEEE Communications Magazine*, vol. 59, no. 8, pp. 107–113, 2021.

[15] Y. Xie, Q. Wu, P. Fan, N. Cheng, W. Chen, J. Wang, and K. B. Letaief, "Resource allocation for twin maintenance and task processing in vehicular edge computing network," *IEEE Internet of Things Journal*, vol. 12, no. 15, pp. 32 008–32 021, 2025.

[16] A. Molina-Galan, L. Lusvarghi, B. Coll-Perales, J. Gozalvez, and M. L. Merani, "On the impact of re-evaluation in 5g nr v2x mode 2," *IEEE Transactions on Vehicular Technology*, vol. 73, no. 2, pp. 2669–2683, 2023.

[17] M. M. Saad, M. A. Tariq, J. Seo, M. Ajmal, and D. Kim, "Age-of-information aware intelligent mac for congestion control in nr-v2x," in *2023 Fourteenth International Conference on Ubiquitous and Future Networks (ICUFN)*. IEEE, 2023, pp. 265–270.

[18] J. Chu, Q. Wu, P. Fan, W. Chen, K. Wang, N. Cheng, and K. B. Letaief, "V2x-assisted distributed computing and control framework for connected and automated cavs under ramp merging scenario," *IEEE Transactions on Mobile Computing*, pp. 1–18, 2026.

[19] T. T. Nguyen, K. Elbassioni, N. C. Luong, D. Niyato, and D. I. Kim, "Access management in joint sensing and communication systems: Efficiency versus fairness," *IEEE Transactions on Vehicular Technology*, vol. 71, no. 5, pp. 5128–5142, 2022.

[20] F. Mehmeti and W. Kellerer, "Max-min fair resource allocation in sd-ran," in *Proceedings of the 18th ACM International Symposium on QoS and Security for Wireless and Mobile Networks*, ser. Q2SWinet '22. New York, NY, USA: Association for Computing Machinery, 2022, p. 27–35. [Online]. Available: https://doi.org/10.1145/3551661.3561359

[21] T. Wang and R. Adve, "Fair licensed spectrum sharing between two mnos using resource optimization in multi-cell multi-user mimo networks," *IEEE Transactions on Wireless Communications*, vol. 21, no. 8, pp. 6714–6730, 2022.

[22] A. Rolich, M. Yildiz, I. Turcanu, A. Vinel, and A. Baiocchi, "On the trade-off between aoi performance and resource reuse efficiency in 5g nr v2x sidelink," in *2025 IEEE Vehicular Networking Conference (VNC)*. IEEE, 2025, pp. 1–8.

[23] A. Rolich, I. Turcanu, and A. Baiocchi, "Aoi-aware and persistence-driven congestion control in 5g nr-v2x sidelink communications," in *2024 22nd Mediterranean Communication and Computer Networking Conference (MedComNet)*. IEEE, 2024, pp. 1–4.

[24] E. Markova, V. Manaeva, E. Zhbankova, D. Moltchanov, P. Balabanov, Y. Koucheryavy, and Y. Gaidamaka, "Performance-utilization trade-offs for state update services in 5g nr systems," *IEEE Access*, 2024.

[25] X. Wang, K. Chen, K. Li, and Q. Yang, "Aoi-aware data propagation in edge computing assisted nr-v2x networks," in *Proceedings of the 6th Asia-Pacific Workshop on Networking*, 2022, pp. 103–104.

[26] S. Song, Z. Zhang, Q. Wu, P. Fan, and Q. Fan, "Joint optimization of age of information and energy consumption in nr-v2x system based on deep reinforcement learning," *Sensors*, vol. 24, no. 13, p. 4338, 2024.

[27] A. Rolich, I. Turcanu, and A. Baiocchi, "Aoi-aware and persistence-driven congestion control in 5g nr - v2x sidelink communications," in *2024 22nd Mediterranean Communication and Computer Networking Conference (MedComNet)*, 2024, pp. 1–4.

[28] Z. Shao, Q. Wu, P. Fan, N. Cheng, Q. Fan, and J. Wang, "Semantic-aware resource allocation based on deep reinforcement learning for 5g-v2x hetnets," *IEEE Communications Letters*, vol. 28, no. 10, pp. 2452–2456, 2024.

[29] X. Xu, Q. Wu, P. Fan, K. Wang, N. Cheng, W. Chen, and K. B. Letaief, "Enhanced velocity-adaptive scheme: Joint fair access and age of information optimization in vehicular networks," *IEEE Transactions on Mobile Computing*, pp. 1–18, 2025.

[30] Q. Wu, Z. Wan, Q. Fan, P. Fan, and J. Wang, "Velocity-adaptive access scheme for mec-assisted platooning networks: Access fairness via data freshness," *IEEE Internet of Things Journal*, vol. 9, no. 6, pp. 4229–4244, 2021.

[31] W. Qiong, S. Shuai, W. Ziyang, F. Qiang, F. Pingyi, and Z. Cui, "Towards v2i age-aware fairness access: A dqn based intelligent vehicular node training and test method," *Chinese Journal of Electronics*, vol. 32, no. 6, pp. 1230–1244, 2023.

[32] W. Zhang, Y. Wang, M. Chen, T. Luo, and D. Niyato, "Optimization of image transmission in cooperative semantic communication networks," *IEEE Transactions on Wireless Communications*, vol. 23, no. 2, pp. 861–873, 2023.

[33] K. Tang, Y. Niu, J. Huang, J. Shi, and H. Zhang, "Unbiased scene graph generation from biased training," in *2020 IEEE/CVF Conference on Computer Vision and Pattern Recognition (CVPR)*, 2020, pp. 3713–3722.

[34] H. Xie, Z. Qin, G. Y. Li, and B.-H. Juang, "Deep learning enabled semantic communication systems," *IEEE Transactions on Signal Processing*, vol. 69, pp. 2663–2675, 2021.

[35] I. Selek, J. Vasara, and E. Ikonen, "Generalized orthogonalization: a unified framework for gram–schmidt orthogonalization, svd and pca," in *2022 IEEE International Conference on Systems, Man, and Cybernetics (SMC)*, 2022, pp. 1754–1759.

[36] S. Kirthiga and M. Jayakumar, "Autoregressive channel modeling and estimation using kalman filter for downlink lte systems," in *Proceedings of the 1st Amrita ACM-W Celebration on Women in Computing in India*, ser. A2CWiC '10. New York, NY, USA: Association for Computing Machinery, 2010. [Online]. Available: https://doi.org/10.1145/1858378.1858423

[37] C. Brady, L. Cao, and S. Roy, "Modeling of nr c-v2x mode 2 throughput," in *2022 IEEE International Workshop Technical Committee on Communications Quality and Reliability (CQR)*. IEEE, 2022, pp. 19–24.

[38] R. Krishna, Y. Zhu, O. Groth, J. Johnson, K. Hata, J. Kravitz, S. Chen, Y. Kalantidis, L.-J. Li, D. A. Shamma, M. S. Bernstein, and F.-F. Li, "Visual genome: Connecting language and vision using crowdsourced dense image annotations," 2016. [Online]. Available: https://arxiv.org/abs/1602.07332

[39] A. Maatouk, M. Assaad, and A. Ephremides, "On the age of information in a csma environment," *IEEE/ACM Transactions on Networking*, vol. 28, no. 2, pp. 818–831, 2020.

[40] R. D. Yates and S. K. Kaul, "The age of information: Real-time status updating by multiple sources," *IEEE Transactions on Information Theory*, vol. 65, no. 3, pp. 1807–1827, 2019.

[41] M. C. Lucas-Estañ, B. Coll-Perales, T. Shimizu, J. Gozalvez, T. Higuchi, S. Avedisov, O. Altintas, and M. Sepulcre, "An analytical latency model and evaluation of the capacity of 5G NR to support V2X services using V2N2V communications," *IEEE Transactions on Vehicular Technology*, vol. 72, no. 2, pp. 2293–2306, 2022.

[42] 3GPP, "Release 16 Description; Summary of Rel-16 Work Items," 3rd Generation Partnership Project (3GPP), Technical report (TR) 21.916, 04 2020, version 16.2.0. [Online]. Available: https://portal.3gpp.org/desktopmodules/Specifications/SpecificationDetails.aspx?specificationId=3493

[43] A. Molina-Galan, L. Lusvarghi, B. Coll-Perales, J. Gozalvez, and M. L. Merani, "On the impact of re-evaluation in 5g nr v2x mode 2," *IEEE Transactions on Vehicular Technology*, vol. 73, no. 2, pp. 2669–2683, 2024.

[44] A. Beck, A. Ben-Tal, and L. Tetruashvili, "A sequential parametric convex approximation method with applications to nonconvex truss topology design problems," *Journal of Global Optimization*, vol. 47, no. 1, pp. 29–51, 2010.

[45] F. Liu, X. Lin, S. Yao, Z. Wang, X. Tong, M. Yuan, and Q. Zhang, "Large language model for multiobjective evolutionary optimization," in *International Conference on Evolutionary Multi-Criterion Optimization*. Springer, 2025, pp. 178–191.

[46] S. Boyd, N. Parikh, E. Chu, B. Peleato, and J. Eckstein, "Distributed optimization and statistical learning via the alternating direction method of multipliers," *Foundations and Trends® in Machine Learning*, vol. 3, no. 1, pp. 1–122, 2011. [Online]. Available: http://dx.doi.org/10.1561/2200000016

[47] R. T. Marler and J. S. Arora, "The weighted sum method for multi-objective optimization: new insights," *Structural and multidisciplinary optimization*, vol. 41, no. 6, pp. 853–862, 2010.

[48] V. L. Vachhani, V. K. Dabhi, and H. B. Prajapati, "Survey of multi objective evolutionary algorithms," in *2015 International Conference on Circuits, Power and Computing Technologies [ICCPCT-2015]*, 2015, pp. 1–9.

[49] J. Blank and K. Deb, "pymoo: Multi-objective optimization in python," *IEEE Access*, vol. 8, pp. 89 497–89 509, 2020.

[50] S. Diamond and S. Boyd, "CVXPY: A Python-embedded modeling language for convex optimization," *Journal of Machine Learning Research*, 2016, to appear. [Online]. Available: https://stanford.edu/~boyd/papers/pdf/cvxpy_paper.pdf

Xiao Xu received the B.S.degree at Jiangnan University. He is currently working toward the M.S.degree form the School of Internet of Things Engineering, Jiangnan University, Wuxi, China. His current research interests include large language model, fair access, muti-objective optimization and age of information in the vehicular network.

Qiong Wu (Senior Member, IEEE) received the Ph.D. degree in information and communication engineering from National Mobile Communications Research Laboratory, Southeast University, Nanjing, China, in 2016. From 2018 to 2020, he was a postdoctoral researcher with the Department of Electronic Engineering, Tsinghua University, Beijing, China. He is currently an associate professor with the School of Internet of Things Engineering, Jiangnan University, Wuxi, China. Dr. Wu is a Senior Member of IEEE and China Institute of Communications. He has published over 80 papers in high impact journals and conferences, and authorized over 30 patents. He was elected as one of the world's top 2% scientists in 2024 and 2022 by Stanford University. He has received the young scientist award for ICCCS'24 and ICITE'24. He won the high-impact paper of Chinese Journal of Electronics award. He has been awarded the National Academy of Artifical Intelligence (NAAI) Certified AI Senior Engineer, and was the excellent reviewer for Computer Networks in 2024. He has severed as the editorial board member of Sensors and CMC-Computers Materials & Continua, the early career editorial board member of Radio Engineering and Chinese Journal on Internet of Things, the lead guest editor of Sensors, CMC-Computers Materials & Continua, Radio Engineering and Frontiers in Space Technologies, the guest editor of Electronics and Chinese Journal on Internet of Things, the TPC co-chair of WCSP'22, the workshop chair of NCIC'23/25, ICFEICT'24/25, CIoTSC'24, IAIC'24, RFAT'25 and FRSE'25, as well as the TPC member and session chair for over 10 international Conferences. His current research interest focuses on vehicular networks, autonomous driving communication technology, and machine learning.

Dr. Pingyi Fan is a professor and the director of open source data recognition innovation center, Department of Electronic Engineering, Tsinghua University. He is member (Academician) of the united states national academy of artificial intelligence (NAAI), Fellow of IET and IET Fellowship international Assessor. He received Ph.D. degree at the Department of Electronic Engineering of Tsinghua University in 1994. From 1997 to 1999, he visited the Hong Kong University of Science and Technology and the University of Delaware in the United States. He also visited many universities and research institutes in the United States, Europe, Japan, Hong Kong and Singapore. He has obtained many research grants, including national 973 Project, 863 Project, mobile special project and the key R&D program, national natural funds and international cooperation projects. He has published more than 600 papers (ORCID) including 171 IEEE journals and more than 10 ESI highly cited papers as well as 4 academic books. He also applied for more than 40 national invention patents, 7 international patents. He won 2025 NAAI AI Exploration Award, and 10 best paper awards of IEEE international conferences, including IEEE ICCCS2023 and 2024, ICC2020 and Globecom 2014, and received the best paper award of IEEE TAOS Technical Committee in 2020, the excellent editor award of IEEE TWC (2009), the most popular scholar award 2023 of AEIC, the second natural Prize of CIC (2023) and several international innovation exhibition medals, i.e. Gold Medal at the Russian Invention Exhibition-2024, Silver Medal at Geneva Invention Exhibition-2023, and Silver Medal at Paris Invention Exhibition-2023 etc. and served as the editorial board member of several Journals, including IEEE and MDPI. He is currently an Associate Editor of IEEE Transactions on Cognitive Communications and Networking (TCCN), the editorial board member of Open Journal of Mathematical Sciences and IAES international journal of artificial intelligence, the deputy director of China Information Theory society, the Co-chair of China's 6G-ANA TG4, and the chairman of Network and Communication Technology Committee of IEEE ChinaSIP. His current research interests are in 6G wireless communication network and machine learning, semantic information theory and generalized information theory, big data processing theory, intelligent network and system detection, etc.

Kezhi Wang received the Ph.D. degree from the University of Warwick, U.K. He is a Professor with the Department of Computer Science, Brunel University of London, U.K. His research interests include wireless communications, mobile edge computing, and machine learning. He is a Clarivate Highly Cited Researcher in 2023-2024.

Nan Cheng (Senior Member, IEEE), received the B.E. and M.S. degrees from the College of Electronics and Information Engineering, Tongji University, Shanghai, China, in 2009 and 2012, respectively, and the Ph.D. degree from the Department of Electrical and Computer Engineering, University of Waterloo, Waterloo, ON, Canada, in 2016. He was a Postdoctoral Fellow with the Department of Electrical and Computer Engineering, University of Toronto, Toronto, ON, Canada, from 2017 to 2019. He is currently a Professor with the State Key Laboratory of ISN and with the School of Telecommunications Engineering, Xidian University, Xi'an, Shaanxi, China. He has published over 90 journal papers in IEEE Transactions and other top journals. His current research focuses on B5G/6G, AI-driven future networks, and space–air-ground integrated networks. Prof. Cheng serves as an Associate Editor for IEEE Transactions on Vehicle Technology, IEEE Open Journal of the Communication Society, and Peer-to-Peer Networking and Applications, and serves/served as a guest editor for several journals.

Wen Chen (M'03–SM'11) received BS and MS from Wuhan University, China in 1990 and 1993 respectively, and PhD from University of Electro-communications, Japan in 1999. He is now a tenured Professor with the Department of Electronic Engineering, Shanghai Jiao Tong University, China, where he is the director of Broadband Access Network Laboratory. He is a fellow of Chinese Institute of Electronics and the distinguished lecturers of IEEE Communications Society and IEEE Vehicular Technology Society. He is the Shanghai Chapter Chair of IEEE Vehicular Technology Society, a vice president of Shanghai Institute of Electronics, Editors of IEEE Transactions on Wireless Communications, IEEE Transactions on Communications, IEEE Access and IEEE Open Journal of Vehicular Technology. His research interests include multiple access, wireless AI and RIS communications. He has published more than 200 papers in IEEE journals with citations more than11,000 in Google scholar.

Khaled Ben Letaief (Fellow, IEEE) received the B.S. (Hons.), M.S., and Ph.D. degrees in electrical engineering from Purdue University, West Lafayette, IN, USA, in December 1984, August 1986, and May 1990, respectively.

From 1990 to 1993, he was a Faculty Member with The University of Melbourne, Melbourne, VIC, Australia. Since 1993, he has been with The Hong Kong University of Science and Technology (HKUST), Hong Kong, where he is currently the New Bright Professor of Engineering. At HKUST, he has held many administrative positions, including an Acting Provost, the Dean of Engineering, the Head of the Electronic and Computer Engineering Department, and the Director of the Hong Kong Telecom Institute of Information Technology. He is an internationally recognized leader in wireless communications and networks. His research interests include artificial intelligence, mobile cloud and edge computing, tactile Internet, and sixth-genereation (6G) systems. In these areas, he has over 720 articles with over 44,450 citations and an H-index of over 100 along with 15 patents, including 11 U.S. inventions.

Dr. Letaief served as a member for the IEEE Board of Directors from 2022 to 2023. He is a member of the National Academy of Engineering, USA, and the Hong Kong Academy of Engineering Sciences; and a Fellow of the Hong Kong Institution of Engineers. He is well recognized for his dedicated service to professional societies and IEEE, where he served in many leadership positions, including the President of the IEEE Communications Society from 2018 to 2019, the world's leading organization for communications professionals with headquarter in New York City, and members in 162 countries. He is recognized by Thomson Reuters as an ISI Highly Cited Researcher and was listed among the 2020 top 30 of AI 2000 Internet of Things Most Influential Scholars. He was a recipient of many distinguished awards and honors, including the 2007 IEEE Communications Society Joseph LoCicero Publications Exemplary Award, the 2009 IEEE Marconi Prize Award in Wireless Communications, the 2010 Purdue University Outstanding Electrical and Computer Engineer Award, the 2011 IEEE Communications Society Harold Sobol Award, the 2016 IEEE Marconi Prize Paper Award in Wireless Communications, the 2016 IEEE Signal Processing Society Young Author Best Paper Award, the 2018 IEEE Signal Processing Society Young Author Best Paper Award, the 2019 IEEE Communication Society and Information Theory Society Joint Paper Award, the 2021 IEEE Communications Society Best Survey Paper Award, and the 2022 IEEE Communications Society Edwin Howard Armstrong Achievement Award. He is the Founding Editor-in-Chief of the prestigious IEEE TRANSACTIONS ON WIRELESS COMMUNICATIONS. He has been involved in organizing many flagship international conferences.